



HAL
open science

Analysis of the equilibrium phase in immune-controlled tumors predicts best strategies for cancer treatment

Kevin Atsou, Sokchea Khou, Fabienne Anjuère, Veronique Braud, Thierry Goudon

► To cite this version:

Kevin Atsou, Sokchea Khou, Fabienne Anjuère, Veronique Braud, Thierry Goudon. Analysis of the equilibrium phase in immune-controlled tumors predicts best strategies for cancer treatment. 2021. hal-03115518

HAL Id: hal-03115518

<https://hal.science/hal-03115518>

Preprint submitted on 19 Jan 2021

HAL is a multi-disciplinary open access archive for the deposit and dissemination of scientific research documents, whether they are published or not. The documents may come from teaching and research institutions in France or abroad, or from public or private research centers.

L'archive ouverte pluridisciplinaire **HAL**, est destinée au dépôt et à la diffusion de documents scientifiques de niveau recherche, publiés ou non, émanant des établissements d'enseignement et de recherche français ou étrangers, des laboratoires publics ou privés.

Analysis of the equilibrium phase in immune-controlled tumors predicts best strategies for cancer treatment

Kevin Atsou ¹, Sokchea Khou ^{2,3}, Fabienne Anjuère ², Véronique M. Braud ^{2*†}
and Thierry Goudon ^{1*†}

¹*Univ. Côte d'Azur, Inria, CNRS, LJAD, Parc Valrose, Nice, France*

²*Université Côte d'Azur, CNRS Institut de Pharmacologie Moléculaire et Cellulaire UMR 7275
660 Route des Lucioles, F-06560 Valbonne, France*

³*Department of Cell, Developmental & Cancer Biology Oregon Health & Science University
3181 SW Sam Jackson Park Road, Portland, OR, 97239, USA*

Abstract

Extensive research and clinical trials have improved our understanding of tumor immunology but despite considerable clinical benefits, current immunotherapies only provide durable responses in a minority of patients. The challenge is to identify key biological parameters preventing immune escape and maintaining an equilibrium state characterized by a stable subclinical tumor mass. Based on a space and size structured partial differential equation model, we developed numerical methods to predict the parameters of the equilibrium without running simulations of the evolution problem. By using global sensitivity analysis methods, we identified the elimination rate of tumor cells by immune cells as the leading parameter influencing the equilibrium size of the tumor and combined therapies that sustain and strengthen the anti-tumor immune response as most effective. Applied to the biological parameters that define a cancer type, such numerical investigation can provide hints for the design and optimization of cancer treatments.

Significance: Based on a space and size structured PDE model, the analyses of the equilibrium phase in immune surveillance of cancer provide numerical methods to evaluate the influence of immune response and tumor growth parameters and hints for the design and optimization of cancer treatments.

1 **Keywords:** cancer, equilibrium phase, immunotherapy,
2 mathematical model, drug response
3

4 Introduction

5 The immune system plays a major role in the control of tu-
6 mor growth. This has led to the concept of immune surveil-
7 lance and cancer immunoediting composed of three phases
8 [1]: the elimination, when tumors are rapidly eradicated by
9 the immune system, the equilibrium, a latency period when
10 tumors can survive but remain on a controlled state, and the
11 escape, the final outgrowth of tumors that have outstripped
12 immunological restraints. In this later phase, immune sup-
13 pression is prevailing and immune cells are also subverted
14 to promote tumor growth. Numerous cancer immunother-
15 apy strategies have been designed and assessed to counter-
16 act cancer immune evasion and restore effective and durable
17 elimination of tumors [2–6] They show improved efficacy over

18 conventional anticancer treatments but only a minority of
19 patients respond. The challenge to face now is to identify
20 key biological parameters which will convert a fatal outcome
21 into a chronic, manageable state, the durable maintenance of
22 cancer in a viable equilibrium phase controlled by immunity.
23 Reaching an equilibrium stage in immune-controlled tumors
24 is indeed the first key step for successful control of tumor
25 growth and a goal for immunotherapy. It is however diffi-
26 cult to apprehend experimentally because the tumor mass at
27 equilibrium is below detectable limits [7]. Mathematical mod-
28 eling of the tumor-immune system interactions offers useful
29 information about the features of the equilibrium phase dur-
30 ing primary tumor development, and can guide the design of
31 optimal anticancer therapies [8–11].

32 We previously [8] introduced a specific mathematical model
33 based on partial differential equations, intended to describe
34 the earliest stages of tumor-immune system interactions. The
35 originality of the model is to introduce size-space structured
36 quantities, providing new perspectives compared to mere or-
37 dinary differential systems [9, 12–14]. The model thus ac-
38 counts for both the growth of the tumor, by natural cell

*Corresponding author. E-mail: braud@ipmc.cnrs.fr,
thierry.goudon@inria.fr

†V. M. Braud and T. Goudon contributed equally to this article.

39 growth and cell divisions, and the displacement of the im-
 40 mune cells towards the tumor, by means of activation pro-
 41 cesses and chemotaxis effects. The most notable finding is
 42 that an equilibrium state, with residual tumor and active im-
 43 mune cells, can be observed. Thus, mathematical analysis
 44 provides a basis for the explanation of the formation of the
 45 equilibrium. Indeed, the equilibrium can be mathematically
 46 interpreted by means of an eigenproblem coupled to a sta-
 47 tionary diffusion equation with constraint. This observation
 48 permits us to develop an efficient numerical strategy to de-
 49 termine *a priori* the shape of the equilibrium — namely, the
 50 size distribution of the tumor cells and the residual tumor
 51 mass — for a given set of biological tumor and immune cell
 52 parameters. Consequently, the equilibrium state can be com-
 53 puted at low numerical cost since we can avoid the resolution
 54 of the evolution problem on a long time range. The use of this
 55 simple and fast algorithm allows us to address the question
 56 of the sensitivity of the residual mass to the parameters and
 57 to discuss the impact of treatments. This information can
 58 be decisive to design clinical studies and choose therapeutic
 59 strategies. Our work therefore provides a tool for cancer
 60 treatment management.

61 Quick guide to equations: A coupled PDE 62 model for tumor-immune system interactions

63 The principles of the modeling adopted in [8] led to couple
 64 an evolution equation for the size-distribution of the tumor
 65 cells, and a convection-diffusion equation for the activated
 66 immune cells. The two-way coupling arose by the death term
 67 induced by the action of the immune cells on the tumor cells,
 68 and by the activation and the attraction of immune cells to-
 69 wards the tumor, which are determined by the total mass of
 70 the tumor. The unknowns are

- 71 • the size density of tumor cells $(t, z) \mapsto n(t, z)$ so that
 72 the integral $\int_a^b zn(t, z) dz$ gives the volume of the tumor
 73 occupied at time t by cells having their size z in the
 74 interval (a, b) ;
- 75 • the concentration of activated immune cells which are
 76 fighting against the tumor $(t, x) \mapsto c(t, x)$;
- 77 • the concentration of chemical signal that attracts the im-
 78 mune cells towards the tumor microenvironment $(t, x) \mapsto$
 79 $\phi(t, x)$.

80 The model assumes that the tumor is located at the center of
 81 a domain Ω , and it distinguishes two distinct length scales.
 82 The size of the tumor cells $z \geq 0$ is considered as “infinitely
 83 small” compared to the scale of displacement of the immune
 84 cells, described by the space variable $x \in \Omega$. Immune cells,
 85 once activated, are subjected to natural diffusion and to a
 86 chemotactic drift, induced by the presence of the tumor. The
 87 strength of this drift, as well as the activation of immune cells,
 88 directly depends on the total mass of the tumor, proportional

89 to the quantity

$$\mu_1(t) = \int_0^\infty zn(t, z) dz.$$

The immune system-tumor competition is described by the following system of PDEs

$$\partial_t n + \partial_z(Vn) = Q(n) - m(n, c), \quad (1a)$$

$$\partial_t c + \nabla_x \cdot (c\chi \nabla_x \phi - D\nabla_x c) = \mu_1 R - \gamma c, \quad (1b)$$

$$- \mathcal{K} \Delta_x \phi = \mu_1 \left(\sigma(x) - \frac{1}{|\Omega|} \int_\Omega \sigma(y) dy \right), \quad (1c)$$

$$n(t, 0) = 0, \quad c|_{\partial\Omega} = 0, \quad \mathcal{K} \nabla_x \phi \cdot \nu(\cdot)|_{\partial\Omega} = 0, \quad (1d)$$

$$n(t = 0, z) = n_0(z), \quad c(t = 0, x) = c_0(x). \quad (1e)$$

90 The growth-division dynamics for the tumor cells (1a) in-
 91 volves the (possibly size-dependent) growth rate $z \mapsto V(z) \geq$
 92 0 and the cell division mechanism is embodied into the op-
 93 erator $Q(n)$. What is crucial for modeling purposes is the
 94 principle that cell-division does not change the total mass:
 95 the operator Q satisfies $\int_0^\infty zQ(n) dz = 0$. However, the total
 96 number of cells in the tumor increases since $\int_0^\infty Q(n) dz \geq 0$
 97 (we refer the reader to [8] for further details). In what follows,
 98 we restrict to the mere symmetric binary division operator

$$Q(n)(t, z) = a(4n(t, 2z) - n(t, z)), \quad (2)$$

99 with $a > 0$ the division rate. Further relevant examples of
 100 division operators can be found in [15]. The boundary condi-
 101 tion for n in (1d) means that no tumor cells are created with
 102 size 0.

103 In the right hand side of (1b), $(t, x) \mapsto R(t, x)$ stands for
 104 the space distribution of the influx rate of activated tumor
 105 antigen specific effector immune cells. It takes into account
 106 the sources of naive immune cells, namely T-cells and NK
 107 cells, that can be activated in the tumor microenvironment
 108 or in the draining lymph nodes into cells fighting the tumor.
 109 The rate of the activation process is supposed to be directly
 110 proportional to μ_1 . The Dirichlet boundary condition for c
 111 in (1d) means that the immune cells far from the tumor are
 112 non-activated. Immune cells are directed towards the tumor
 113 by a chemo-attractive potential ϕ , induced by the presence of
 114 the tumor cells. Through (1c), the strength of the signal is
 115 proportional to the total mass of the tumor, and it is shaped
 116 by a form function $x \mapsto \sigma(x)$. Finally, the activated immune
 117 cells are able to destroy tumor cells, as described by the death
 118 term in (1a)

$$m(c, n)(t, z) = \underbrace{\int_\Omega \delta(y)c(t, y) dy}_{:=\mu_c(t)} \times n(t, z), \quad (3)$$

119 where $\delta \geq 0$ is another form function. For the numerical
 120 experiments, we shall work with the Gaussian profiles

$$\delta(x) = \frac{A}{\theta\sqrt{2\pi}} \exp\left(-\frac{|x|^2}{2\theta^2}\right), \quad \sigma(x) = \frac{A_\sigma}{\theta_\sigma\sqrt{2\pi}} \exp\left(-\frac{|x|^2}{2\theta_\sigma^2}\right). \quad (4)$$

We refer the reader to [8] for further details and comments about the model.

Results

Identification of biological parameters

In order to go beyond the qualitative discussion of [8], the model should be challenged with biological data. The PDE system is governed by the set of parameters collected in **Table 1**: most parameter values were retrieved from previously published experimental results. We propose an estimation of the parameters R, a, V based on the experimental study performed in [16] where the development of chemically-induced cutaneous squamous cell carcinoma (cSCC) is investigated.

To estimate the parameter R , we used a simple linear regression, by using 34 data points from an in vivo experimental cutaneous squamous cell carcinoma (cSCC) tumor growth mouse model [16]: R is predicted from the “influx rate of effector immune cell”, denoted by Y and expressed in $cell_c \cdot day^{-1}$, given as a function, assumed to be linear, of the volume of the tumor μ_1 in μm^3 , see **Fig. 1-(a)**. The determination coefficient and the p-value are respectively, $r^2 = 0.705$ and $p = 2.84 \cdot 10^{-10}$, the slope of the regression line is $R = 7.92 \cdot 10^{-7}$. It is measured in $\frac{cell_c \cdot mm^{-3}}{\mu m^3} \cdot day^{-1}$ assuming homogeneity with respect to the unit mm^3 . **Table 1** gives the 95% confidence interval. This interval is quite small, but it already shows a sensitive impact of variations of this parameter; since the variability due to the biological model is likely important and we wished to investigate the impact of treatments that directly affect this parameter, we also made some simulations with a larger range of values (see for instance **Fig.6**)

We then determined the tumor growth parameters a and V . Neglecting the immune response, the tumor growth is driven by

$$\partial_t n + \partial_z(Vn) = Q(n). \quad (5)$$

As explained below, this leads to an exponential growth of the tumor mass, see [15, 29–31]. Let $t \mapsto \mu_0 = \int_0^\infty n(t, z) dz$ and $t \mapsto \mu_1(t) = \int_0^\infty zn(t, z) dz$. We thus get

$$\frac{d}{dt}\mu_0 = a\mu_0, \quad \frac{d}{dt}\mu_1 = V\mu_0. \quad (6)$$

We now aim at estimating the division rate a and the growth rate V from the experimental data, **Fig. 1-(b,c)**. We denote $\Theta = (a, V)$ the parameters to be identified. We have at hand some experimental noisy data $(Y_1^{(0)}, \dots, Y_n^{(0)})$, $(Y_1^{(1)}, \dots, Y_n^{(1)})$ representing respectively μ_0 and μ_1 at several times. Hence, we have

$$Y_i^{(j)} = \mu_{j,\Theta}(t_i) + \epsilon_i, \quad i \in \{1, \dots, n\}, \quad j \in \{0, 1\} \quad (7)$$

where $t \mapsto (\mu_{0,\Theta}, \mu_{1,\Theta})(t)$ stands for the solution of (6) defined with the parameters Θ . Forgetting for a while the discreteness of the observed data, the approach can be expressed

as a cost minimization problem where the cost function is defined by

$$C_\lambda^{(j)}(\Theta) = \int_0^T |\mu_{j,\Theta}(t) - Y^{(j)}(t)|^2 dt. \quad (8)$$

We finally set

$$\hat{\Theta} = \operatorname{argmin}\{C_\lambda^{(j)}(\Theta), \Theta = (a, V), a > 0, V > 0\}. \quad (9)$$

We fit the data that give the number of cells in the tumor and the volume of the tumor for several times by using a non-linear least square algorithm, the Levenberg-Marquardt algorithm [32], [33], **Fig. 1-(d,e)**.

Development of numerical methods predicting parameters of the equilibrium in immune-controlled tumors

Based on the space and size structured PDE model (1a)-(1e), we studied the equilibrium phase in immune-controlled tumors. We wished to predict, for given biological parameters, see **Table 1**, the total mass of the residual tumor and its size distribution. To this end, we developed specific numerical procedures based on the mathematical interpretation of the equilibrium.

Equilibrium states

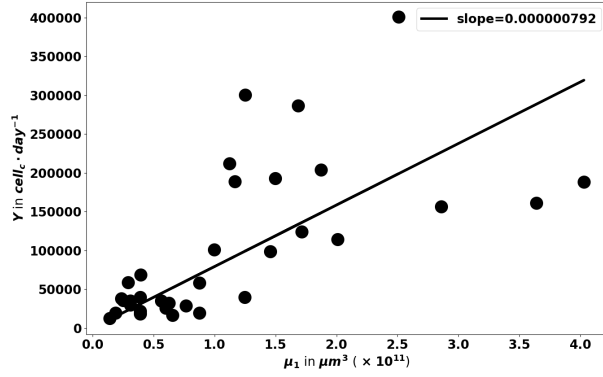
The definition of the equilibrium relies on the following arguments. The cell-division equation admits a positive eigenstate: in absence of immune response, see (5), the tumor population grows exponentially fast, with a rate $\lambda > 0$, and its size repartition obeys a certain profile \bar{N} . The equilibrium occurs when the immune response counterbalances the growth rate of this equation. To be more specific, we look for $\lambda > 0$ and a non negative function $z \geq 0 \mapsto \bar{N}(z)$ satisfying

$$\begin{cases} \partial_z(V\bar{N}) - Q(\bar{N}) + \lambda\bar{N} = 0 \text{ for } z \geq 0 \\ \bar{N}(0) = 0, \quad \bar{N}(z) > 0 \text{ for } z > 0, \quad \int_0^{+\infty} \bar{N}(z) dz = 1. \end{cases} \quad (10)$$

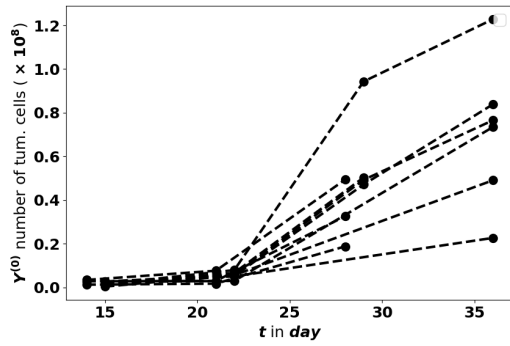
The existence-uniqueness of the eigenpair (λ, \bar{N}) can be found in [15, 29]. When the tumor does not interact with the immune system, the large time behavior is precisely driven by the eigenpair: the solution of (5) behaves like $n(t, z) \sim_{t \rightarrow \infty} \nu_0 e^{\lambda t} \bar{N}(z)$ where ν_0 is a constant determined by the initial condition, see [29, 30]. In the specific case where V is constant and Q is the binary division operator (2), we have $\lambda = a$ and the profile \bar{N} is explicitly known, [31, 34]. However, for general growth rates and division kernels the solution should be determined by numerical approximations.

Coming back to the coupled model, we infer that the equilibrium phase corresponds to the situation where the death rate precisely counterbalances the natural exponential growth of the tumor cell population. In other words, the equilibrium is defined by the stationary equation

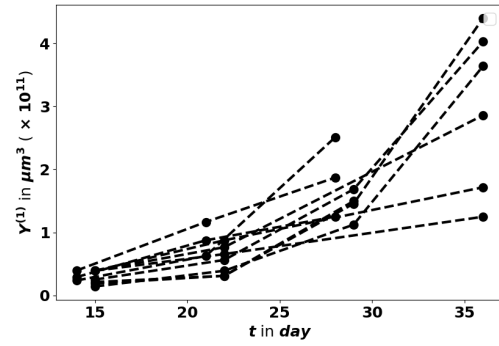
$$\gamma C - \nabla_x \cdot (D \nabla_x C) - \mu_1 \nabla_x \cdot (\chi C \nabla_x \Phi) = g(\mu_1)R, \quad C|_{\partial\Omega=0} = 0, \quad (11)$$



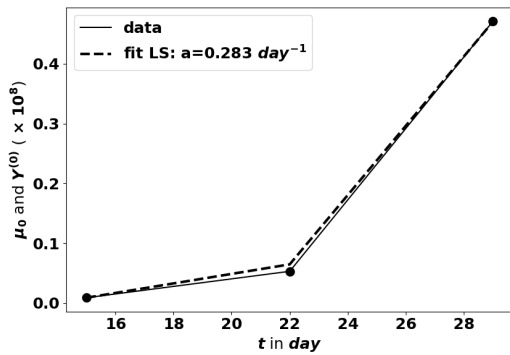
(a) influx rate of effector immune cell



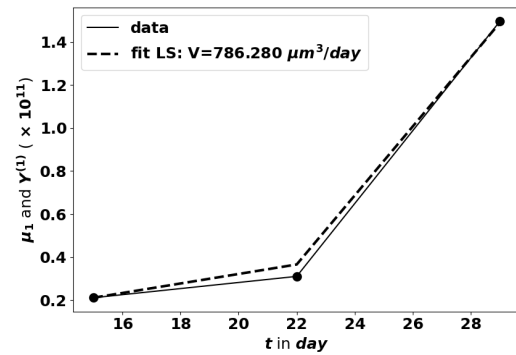
(b) tumor cell number



(c) tumor volume



(d) curve fit of tumor cell number



(e) curve fit of tumor volume

Figure 1. (a): Regression on the “influx rate of effector immune cell” Y (in $cell_c \cdot day^{-1}$) as a function of the tumor volume μ_1 in μm^3 (b) and (c): Tumor evolution kinetics from in vivo experimental cSCC tumor growth in mice. (d) and (e): Illustration of the estimation of the parameters a and V : $a = 0.283 \text{ day}^{-1}$ and $V = 786.280 \mu m^3 \cdot day^{-1}$ using 3 data points of a typical tumor evolution kinetic, from the dataset depicted in (b) and (c)

Symbol	Description	Value and unit	References
χ	chemotactic coefficient	$8.64 \times 10^1 - 8.64 \times 10^6$ $mm^2 \cdot mmol^{-1} \cdot day^{-1}$	(Macrophages) [17]
D	natural space diffusion coef. of the cytotoxic effector cells population	$8.64 \times 10^{-5} - 10^{-3} mm^2 \cdot day^{-1}$	(CD8 ⁺ T-cells) [18], [19]
R	the normal rate of influx of effector immune cells	$6.11 \times 10^{-7}, 9.74 \times 10^{-7}$ $\frac{cell \cdot mm^{-3}}{\mu m^3} \cdot day^{-1}$	estimated
γ	natural death rate of the tumor antigen-specific cytotoxic effector cells	$2 \times 10^{-2} - 1 day^{-1}$	[20], [21], [12], [22]
A	strength of the immune response	$2 - 57.6 cell_c^{-1} \cdot day^{-1}$	[23], [24], [25], [26]
\mathcal{K}	natural space diffusion of the attractive potential ϕ	$10^{-2} - 1 mm^2 \cdot day^{-1}$	[27], [19]
A_σ	strength of the chemical signal induced by each tumor cell	$5 \cdot 10^{-17} - 0.625 \times 10^{-16}$ $mmol \cdot^{-1} \mu m^3 \cdot day^{-1}$	[28]
a	division rate of the tumor cells	$0.103 - 0.351 day^{-1}$	estimated
V	growth rate of the tumor cells	$308.526 - 2521.975 \mu m^3 \cdot day^{-1}$	estimated

Table 1. Key model parameters and their biophysical meaning

where Φ is the solution of

$$-\mathcal{K}\Delta_x\Phi = \sigma - \frac{1}{|\Omega|} \int_{\Omega} \sigma(y) dy,$$

endowed with the homogeneous Neumann boundary condition, together with the constraint

$$\int_{\Omega} \delta(x)C(x) dx = \lambda. \quad (12)$$

This can be interpreted as an implicit definition of the total mass μ_1 , to be the value such that the solution of the boundary value problem (11) satisfies (12). The existence of an equilibrium state defined in this way is rigorously justified in [8, Theorem 2]. **Fig. 2** illustrates how the equilibrium establishes in time: as time becomes large, the concentration of active immune cells in the neighborhood of the tumor tends to the eigenvalue of the cell-division equation, the total mass tends to a constant and the size distribution of tumor cells takes the profile of the corresponding eigenstate. This result has been obtained by using the lower bounds of the parameters in **Table 1** for the immune system and $(a, V) = (0.351, 713.608)$ for the tumor growth. We observe a non symmetric shape, peaked about a diameter of $13 \mu m$, which is consistent with

observational data reporting the mean size distribution of cancer cells [35].

Numerical experiments show that the model (1a)–(1e) is able to reproduce, in the long-time range, cancer-persistent equilibrium, but the features of the equilibrium, and its ability to establish, are highly sensitive to the parameters in **Table 1**. To discuss this issue further, we focus here on the mass at equilibrium considered as a critical quantity that evaluates the efficacy of the immune response. Indeed, it is known that a tumor gains in malignancy when its mass reaches certain thresholds [36, 37]. The smaller the tumor mass at equilibrium, the better the vital prognosis of the patient. In doing so, we do not consider transient states and time necessary for the equilibrium to establish (see **Fig. 4-(a-c)**).

The determination, on numerical grounds, of the equilibrium state relies on a two-step process. First, we compute the normalized eigenstate of the tumor cell equation, second, we find the tumor mass which makes the coupled death rate fit with the eigenvalue. To this end, we have developed a specific numerical approach.

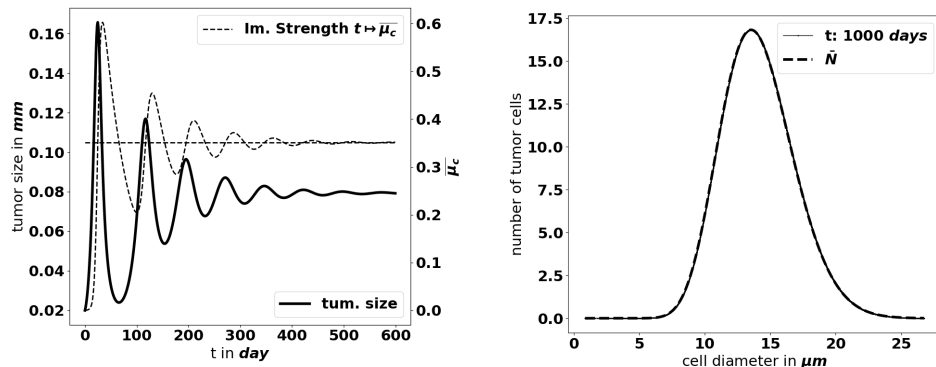


Figure 2. Left: Time evolution of the diameter of the tumor (bold black line) and concentration of active immune cells (dotted gray line). Right: Comparison of the tumor cell-size distribution at $t = 1000$ days with the positive eigenstate of the cell division equation (x-axis: size of the tumor cells, y-axis: number of tumor cells at the final time)

The eigen-elements of the growth-division equation

The numerical procedure is inspired from the spectral analysis of the equation: λ is found as the leading eigenvalue of a conveniently shifted version of the growth-division operator. In practice, we work with a problem where the size variable is both truncated and discretized. Hence, the problem recasts as finding the leading eigenvalue of a shifted version of the underlying matrix, which can be addressed by using the inverse power method [38, Section 1.2.5]. We refer the reader to [39, 40] for a thorough analysis of the approximation of eigenproblems for differential and integral operators, which provides a rigorous basis to this approach. It is also important to check a priori, based on the analysis of the equation [15], how large the shift should be, and that it remains independent on the numerical parameters, see Suppl. Material. For some specific fragmentation kernels and growth rates, the eigenpair (λ, N) is explicitly known, see [15]. We used these formula to validate the ability of the algorithm to find the expected values and profiles, see Suppl. Material.

Computation of the equilibrium mass

Having at hand the eigenvalue λ , we go back to the convection-diffusion equation (11) and the constraint (12) that determine implicitly the total mass μ_1 of the residual tumor. For a given value of μ_1 , we numerically solve (11) by using a finite volume scheme, see [8, Appendix C]. Then, we use the dichotomy algorithm to fit the constraint:

- The chemo-attractive potential Φ is computed once for all.
- Pick two reference values $0 < \mu_a < \mu_b$; the mass we are searching for is expected to belong to (μ_a, μ_b) .
- Set $\mu_1 = \frac{\mu_a + \mu_b}{2}$ and compute the associated solution C_{μ_1} of (11). Evaluate the discrete version of $I = \int \delta C_{\mu_1} dx - \lambda$.

- If $I < 0$, then replace μ_a by μ_1 , otherwise replace μ_b by μ_1 .
- We stop the algorithm when the relative error $\frac{\mu_b - \mu_a}{\mu_a} < \epsilon$ is small enough.

It is also possible to design an algorithm based on the Newton method. However, this approach is much more numerically demanding (it requires to solve more convection-diffusion equations) and does not provide better results.

For the evaluation of the residual mass, we do not know explicit solutions, even for the simplest model. Nevertheless, we can compare the results of the inverse power-dichotomy procedure that predicts the residual mass, to the large time simulations as performed in [8].

Therefore, we adopt the same framework as in [8]: the tumor is located at the origin of the computational domain Ω , which is the two-dimensional unit disk. We work with the lower bound of the parameters collected in **Table 1**. We compare the asymptotic value of the total mass μ_1^f given by the large time simulation of the evolution problem (and checking that the variation of the total mass has become negligible) to the total mass μ_1^{pd} predicted by the power-dichotomy procedure; let

$$E_{\mu_1} = \frac{|\mu_1^f - \mu_1^{pd}|}{\mu_1^f}.$$

The results for several cell division rates a are collected in **Table 2**: the numerical procedures finds the same equilibrium mass as the resolution of the evolution problem, which is another validation of the method.

Numerical simulations show how parameters influence equilibrium

The numerical methods were next used to assess how the parameters influence the equilibrium. In particular, we wish

a	μ_1^f (mm^3) at final time $T = 500$	μ_1^{pd} (mm^3)	E_{μ_1}
0.103	$7.67271875 \times 10^{-5}$	$7.67271872 \times 10^{-5}$	4.10×10^{-9}
0.15	$1.11701535 \times 10^{-4}$	$1.11701543 \times 10^{-4}$	7.97×10^{-8}
0.20	$1.48924575 \times 10^{-4}$	$1.48924641 \times 10^{-4}$	4.40×10^{-7}
0.3	$2.23420663 \times 10^{-4}$	$2.23420562 \times 10^{-4}$	4.53×10^{-7}
0.351	$2.61368442 \times 10^{-4}$	$2.61367974 \times 10^{-4}$	1.80×10^{-6}

Table 2. Comparison of the large time tumor mass and the predicted tumor mass for several values of a

to assess the evolution of the tumor mass at equilibrium according to immune response and tumor growth parameters.

For the numerical simulations presented here, we thus work on the eigenproblem (10) and on the constrained system (11)-(12). Unless precisely stated, the immune response parameters are fixed to the lower bounds in **Table 1**. The tumor growth parameters are set to $a = 0.3 \text{ day}^{-1}$ and $V = 469.545 \mu m^3 \cdot \text{day}^{-1}$. When necessary, the initial values of the unknowns are respectively $\mu_0(0) = 1 \text{ cell}_n$, $\mu_1(0) = 4188 \mu m^3$, $c(0, x) = 0$.

The main features of the solutions follow the observations made in [8], which were performed with arbitrary “academic” values for the parameters. We observe that $\int_{\Omega} \delta(y)c(t, y) dy$ tends to the division rate a , which in this case corresponds to the leading eigenvalue of the cell-division equation. It is remarkable that the predicted diameter of the tumor at equilibrium — see **Fig. 2** — is significantly below modern clinical PET scanners resolution limit, which could detect tumors with a diameter larger than 7 mm [41]. This is consistent with the standard expectations about the equilibrium phase [7], but, of course, it makes difficult further comparison of the prediction with data.

The aggressiveness of the tumor is characterized by the division rate, the variations of which impact the size of the tumor at equilibrium: the larger a , the larger the residual tumor, see **Fig. 3-(a)**. Increasing the immune strength A increases the efficacy of the immune response, reducing the size of the residual tumor see **Fig. 3-(b)**. Similarly, increasing the mean rate of influx of effector immune cells in the tumor microenvironment R , decreases the tumor size at equilibrium, see **Fig. 3-(c)**. On the contrary, increasing the death rate of the immune cells γ reduces the efficacy of the immune response and increases the equilibrium tumor size see **Fig. 3-(d)**.

Moreover, as mentioned above, not only the parameters determine the equilibrium mass, but they also impact how the equilibrium establishes. **Fig. 4-(a-c)** shows what happens by making the tumor cell division rate a vary. There are more oscillations along time, with larger amplitude, as a increases. Similar observations can be made when reducing the strength of the immune system A (likely out of its realistic range), see **Fig 4-(d-f)**. The smaller A , the weaker the damping of the oscillations and the longer the periods. We notice that the decay of the maximal tumor radius holds at a polynomial

rate. In extreme situations, the equilibrium does not establish on reasonable observation times, and the evolution can be confounded with a periodic alternance of growing and remission phases. Such scenario illustrates that the relevance of the equilibrium can be questionable depending on the value of the parameters. In what follows, we focus on the details of the equilibrium itself, rather than on the transient states.

Global sensitivity analysis on the equilibrium mass identifies the key parameters to target in cancer therapy

Since the equilibrium state can be computed for a reduced numerical cost (it takes about 1/4 of a second on a standard laptop), we can perform a large number of simulations, sampling the range of the parameters. This allows us to discuss in further details the influence of the parameters on the residual mass and, by means of a global sensitivity analysis, to make a hierarchy appear according to the influence of the parameters on this criterion. Ultimately, this study can help in proposing treatments that target the most influential parameters.

Details on the applied methods for the sensitivity analysis can be found in the Suppl. Material. Among the parameters, we distinguish:

- the tumor cell division rate a which drives the tumor aggressiveness,
- the efficacy of the immune system, governed by the mean influx rate of activated effector immune cells R , the strength of the immune response A , the chemotactic sensitivity χ , the death rate γ of the immune cells, and the strength of the chemical signal induced by each tumor cell A_{σ}
- environmental parameters such as the diffusion coefficients D (for the immune cells) and \mathcal{K} (for the chemokine concentration).

We assume that the input parameters are independent random variables. Due to the lack of knowledge on the specific distribution of these parameters and according to the constraints on the parameter bounds (**Table 1**), the most suitable probability distribution is the one which maximizes the continuous entropy ([42]), more precisely, the uniform distribution. Therefore, the uncertainty in the parameter values is represented by uniform distributions $\mathcal{U}(p_{min}, p_{max})$ where

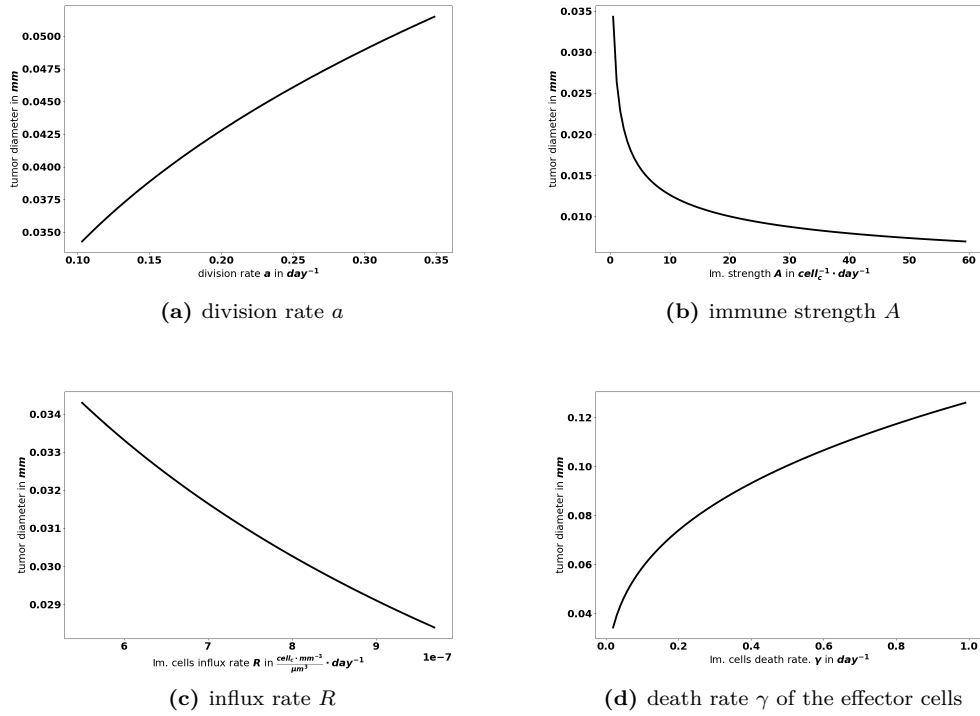


Figure 3. Evolution of the tumor diameter at equilibrium, with respect to the division rate a , the strength of the effector immune cells A , the influx rate of effector immune cells R , the natural death rate γ of the effector cells

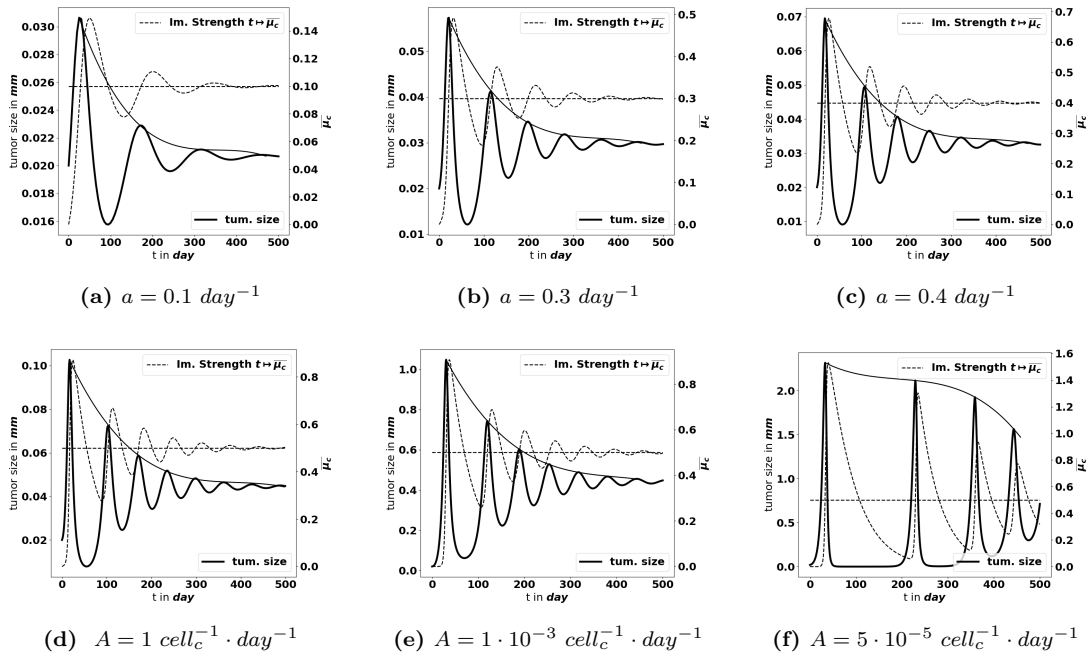


Figure 4. Large-time simulation of the PDE system: evolution of the tumor diameter (bold black line, left axis), and of the concentration of immune cells $\bar{\mu}_c$ (dotted grey line, right axis), for several values of the division rate a (top) and for several values of the immune strength A (bottom). The equilibrium needs more time to establish as the strength of the immune system decreases

p_{min} and p_{max} are respectively the lower and upper bound of each uncertain input parameter (see **Table 1**). In what follows, the total mass at equilibrium, μ_1 , given by the power-dichotomy algorithm, is seen as a function of the uncertain parameters:

$$\mu_1 = f(a, A, R, \chi, D, A_\sigma, \gamma, \mathcal{K}). \quad (13)$$

To measure how the total variance of the output μ_1 of the algorithm is influenced by some subsets $i_1 \dots i_p$ of the input parameters $i_1 \dots i_k$ ($k \geq p$ being the number of uncertain input parameters), we compute the so-called Sobol's sensitivity indices. The total effect of a specific input parameter i is evaluated by the total sensitivity index $S_T^{(i)}$, the sum of the sensitivity indices which contain the parameter i . (Details on the computed Sobol indices can be found in Suppl. Material). The computation of these indices is usually based on a Monte Carlo (MC) method (see [43, 44]) which requires a large number of evaluations of the model due to its slow convergence rate ($O(1/\sqrt{N})$ where N is the size of the experimental sample). To reduce the number of model evaluations, we use instead the so-called generalized Polynomial Chaos (gPC) method (see [45]). The backbone of the method is based on building a surrogate of the original model by decomposing the quantity of interest on a basis of orthonormal polynomials depending on the distribution of the uncertain input parameters $\theta(\omega) = (a, A, R, \chi, D, A_\sigma, \gamma, \mathcal{K})$, where ω represents an element of the set of possible outcomes. Further details on the method can be found in [46]. For uniform distributions, the most suitable orthonormal polynomial basis is the Legendre polynomials. The analysis of the distribution of μ_1 after a suitable sampling of the parameters space indicates that μ_1 follows a log-normal distribution. This distribution is not uniquely determined by its moments (the Hamburger moment problem) and consequently cannot be expanded in a gPC (see [47]). Based on this observation, to obtain a better convergence in the mean square sense, we apply the gPC algorithm on the natural logarithm of the output μ_1 . Typically, $\ln(\mu_1)$ is decomposed as follows:

$$\ln(\mu_1(\omega)) = \sum_{\alpha \in \mathcal{I}_{k,p}} q_\alpha L_\alpha(\theta(\omega)) + \varepsilon, \quad (14)$$

where ε corresponds to the approximation error, $\mathcal{I}_{k,p} = \{\alpha \in \mathbb{N}^k : \sum_{i=1}^k \alpha_i \leq p\}$ and p represents the highest degree of the expansion. Hence, the dimension of the polynomial basis is given by $\frac{(k+p)!}{k!p!}$. We reduce the number of model evaluations to 642 runs by constraining also the parameters interaction order to 2. For our purpose, a degree $p = 5$ gives a better fit (see **Fig. 5-Top**) to the original model and the goodness of fit of the gPC algorithm is measured by a Leave One Out Cross Validation (LOOCV) technique [48]. The resulting LOO error indicates 0.4% prediction error. The Sobol's sensitivity indices are then computed from the exponential of the surrogate model (14) by using Monte Carlo simulations

combined with a careful space-filling sampling of the parameters space (see [43, 49]). For the computations, a sample with $N = 1.8 \times 10^6$ points has been used in order to get stable second order Sobol indices. Indeed, the sensitivity indices that are needed to discriminate the impact of the input parameters are the first and total Sobol' sensitivity indices. Here, the analysis revealed a significant difference between some first order Sobol' indices and their corresponding total Sobol indices, which indicated the importance of computing also the second order Sobol' indices.

It is important to stress that the obtained results, and the associated conclusions, could be highly dependent on the range of the parameter values. This observation makes the measurement / estimation of the parameters a crucial issue which can be dependent on the type of cancer analyzed.

Efficacy of the immune response The first order Sobol indices represented in **Fig. 5-bottom-left** indicate that the parameters which impact the most the variability of the immune-controlled tumor mass at equilibrium are respectively,

- the strength of the lethal action of the immune cells on the tumor cells A ,
- the natural death rate γ of the effector immune cells,
- the division rate a of the tumor cells,
- the influx rate of activated effector immune cells into the tumor microenvironment R .

This is consistent with the observations made from the numerical experiments above and in [8]: the immune response is enhanced by increasing either A or R , and decreasing γ . Surprisingly, the chemotactic sensitivity χ , like the strength of the chemical signal induced by each tumor cell A_σ , the space diffusion coefficient of the effector immune cells D and the diffusion coefficient of the chemokines \mathcal{K} , have a negligible influence on the immune-controlled tumor mass, see **Fig. 5-bottom-left**, whether individually or in combination with other parameters. This result can be explained by the fact that despite the capacity of the cells of the immune system to infiltrate the tumor, this ability has a reduced effect when these cells are not able to effectively kill the tumor cells.

The second order Sobol' indices indicate that the leading interactions are the pairs (A, γ) , (a, A) , (a, γ) and (A, R) . Accordingly, in order to enhance the immune response, an efficient strategy can be to act simultaneously on the immune strength A together with the natural death rate γ or together with tumor division rate a . Increasing the influx rate of activated effector immune cells into the tumor microenvironment R , by enhancing the activation / recruitment processes leading to the conversion of naive immune cells into tumor antigen specific effector immune cells, can also be efficient when combined with an action on A .

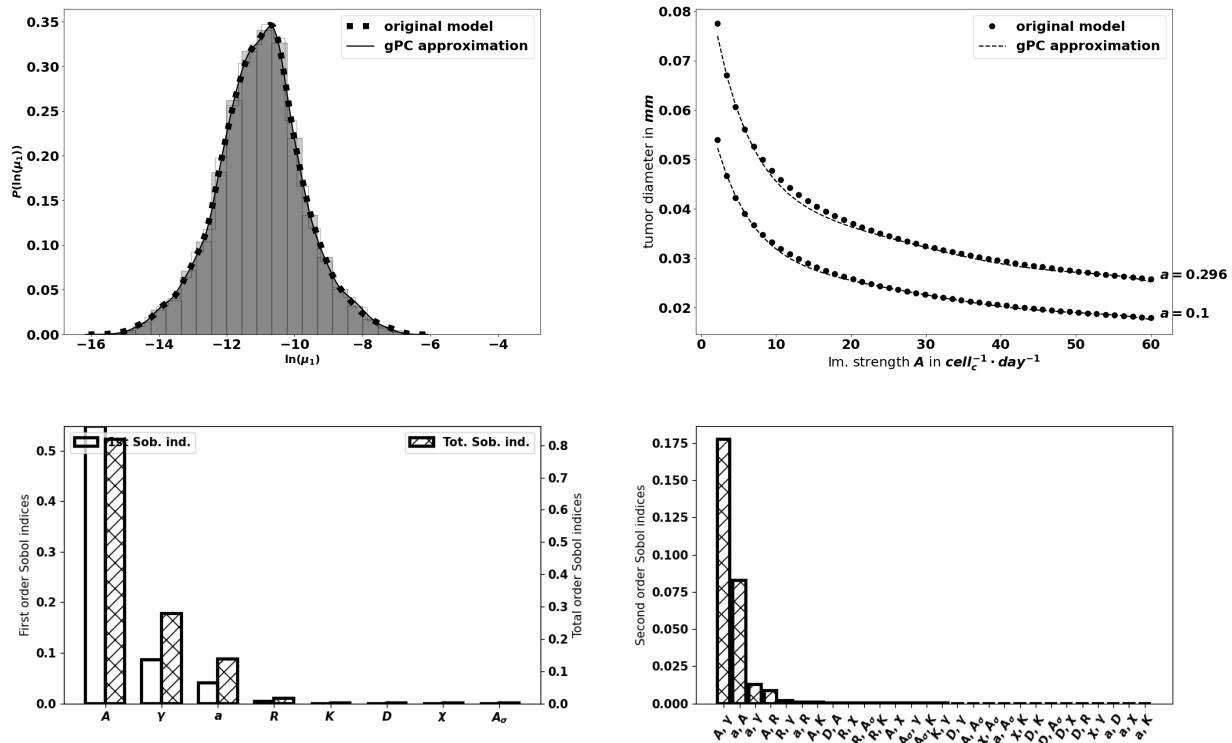


Figure 5. Top-Left: comparison between the pdf of $\ln(\mu_1)$ from the gPC approximation and the pdf from the original model. Top-Right: Comparison between the value of μ_1 generated by the power-dichotomy algorithm and the gPC approximation. Bottom-Left: First (empty) and total (dashed) order Sobol indices for μ_1 . Bottom-Right: Second order Sobol indices for μ_1

The tumor aggressiveness The tumor aggressiveness is mainly described by the cell division rate a . The first order Sobol indice indicates that a influences significantly the tumor mass at equilibrium, and we observe that the total Sobol index of a is higher than the individual one. This indicates that this parameter has strong interactions with the others. By taking a look at **Fig. 5**-bottom-right we remark that a interacts significantly with the parameters A, γ . However, the most significant interaction is the one with A . This is consistent with recent successes of combined therapies targeting tumor and immune cells [50].

Towards optimized treatments Because equilibrium state can be computed for a reduced numerical cost, it allows a large number of simulation to be performed in a minimal time, so that an extensive sampling of the range of the parameters can be tested. The flexibility of the numerical simulations provides valuable tools to assess the efficiency of a variety of therapeutic strategies.

Fig. 6 illustrates how the equilibrium mass is impacted when combining variations of two parameters, namely the immune strength A combined to the tumor cell division rate a , the mean rate of influx of effector immune cells R or the death rate of effector immune cells γ ; and the tumor cell division rate a with the death rate γ . Interestingly, a reduction of the tumor mass at equilibrium can be obtained significantly more easily by acting on two parameters than on a single one. For

instance, reducing the tumor cell division rate a from 0.35 to 0.1 cannot reduce the diameter of the tumor below .025 mm, with $A = 1$; while the final size is always smaller when $A = 3.95$. This observation highlights the interest of combined treatments having such complementary actions. The interest is two-fold: either smaller residual tumors can be obtained by pairing two actions, or the same final tumor size can be obtained with a combined treatment having less toxicity than a mono-therapy.

Conclusion and Discussion

Controlling parameters that maintain cancer-immune equilibrium is key to the successful development of future cancer therapies. To understand how equilibrium establishes and how it is influenced by immune, environmental and tumor-related parameters, we evaluate the tumor mass which tends to a constant at equilibrium. In this study, we make use of the space and size structured mathematical model developed in [8] to provide innovative, efficient methods to predict, at low numerical cost, the residual tumor mass at equilibrium. By means of numerical simulations and global sensitivity analysis, we identify the elimination rate A of tumor cells by immune cells as the most influential factor. Therefore, the most efficient therapeutic strategy is to act primarily on the immune system rather than on the tumor itself. We also demonstrate the need to develop combined cancer treatments,

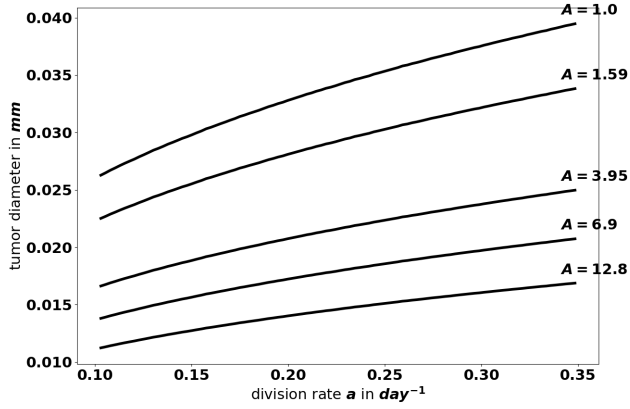
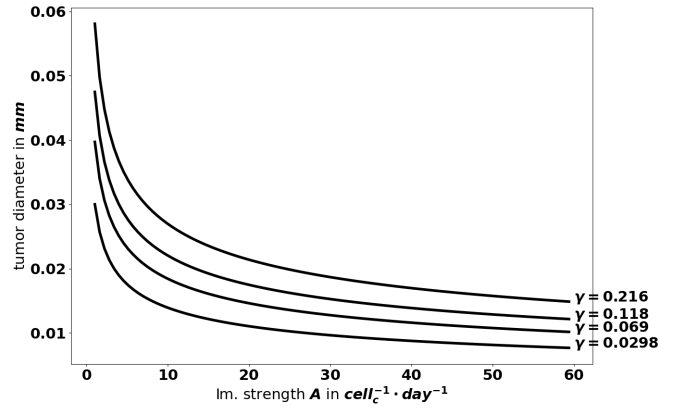
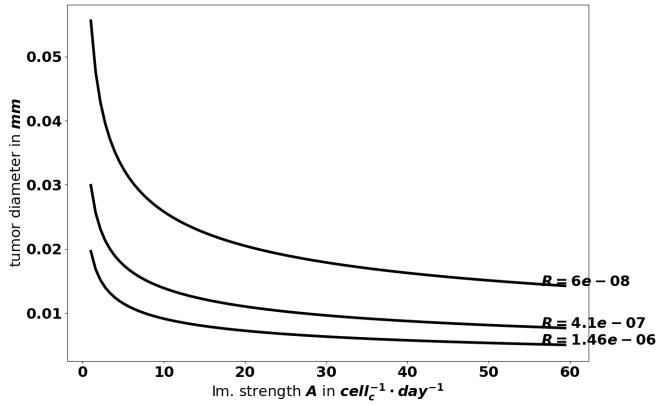
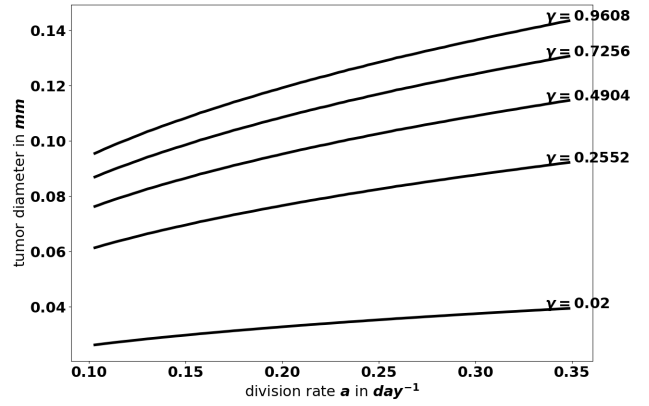

 (a) different values for the pair (a, A)

 (b) different values for the pair (A, γ)

 (c) different values for the pair (A, R)

 (d) different values for the pair (a, γ)

Figure 6. Evolution of the tumor diameter at equilibrium, with respect to the division rate a for several values of the immune strength A (a), with respect to the immune strength A for several values of the death rate γ (b), with respect to the immune strength A for several values of the influx rate of effector immune cells R (c), and with respect to the division rate a for several values of the death rate γ (d).

531 boosting the immune capacity to kill tumor cells (increase
 532 A), reducing natural death rate of effector immune cells (de-
 533 crease γ), boosting the conversion into efficient immune cells
 534 (increase R) and reducing the ability of tumor cells to divide
 535 (decrease a). The combination of such approaches definitely
 536 outperforms the performances of a single action; it permits
 537 to maintain the tumor in a long-lasting equilibrium state, far
 538 below measurement capabilities.

539 Generally, therapeutic strategies are designed to target pre-
 540 formed, macroscopic cancers. Indeed, patients are diagnosed
 541 once their tumor is established and measurable, thus at the
 542 escape phase of the cancer immunoediting process [1]. The
 543 goal of successful treatments is to revert to the equilibrium
 544 phase and ultimately to tumor elimination. Experimental
 545 and clinical evidence indicate that equilibrium exists but it
 546 is difficult to measure, being below detection limit. It is re-
 547 garded as “a tumor mass dormancy” when the rate of cancer
 548 cell proliferation matches their rate of elimination by immune

549 cells. In human, cancer recurrence after therapy and long pe-
 550 riods of remission or detection of low number of tumor cells
 551 in remission phases are suggestive of such equilibrium phase.
 552 Mathematical models can also be used to provide evidence of
 553 such state. The system of partial differential equations pro-
 554 posed in [8] is precisely intended to describe the earliest stages
 555 of immune control of tumor growth. Remarkably, while be-
 556 ing in the most favorable condition, only taking into account
 557 the tumor antigen-specific cytotoxic immune cells and no im-
 558 munosuppressive mechanisms, the model reproduces the for-
 559 mation of an equilibrium phase with maintenance of residual
 560 tumor cells rather than their complete elimination. Besides
 561 suggesting that elimination may be difficult to reach, this
 562 finding also brings out the role of leading parameters that
 563 shape the equilibrium features and opens new perspectives to
 564 elaborate cancer therapy strategies that reach this state of
 565 equilibrium.

To decipher tumor-immune system dynamics leading to

equilibrium state, we have developed here computational tools. The total mass of the tumor is a critical criterion of the equilibrium and was used to predict parameters that contribute the most to the establishment of the equilibrium. By means of global sensitivity analysis, we identified four parameters that affect the most the variability of the immune-controlled tumor mass. Three of them are related to immune cells, A , R and γ and one to tumor cells, a . Moreover, the influence of the leading parameters is significantly increased when they are paired. This observation validates the development of combined therapeutic treatments which would be more efficient at reducing tumor growth and reduce toxicity. Because the pair (a, A) is among the most influential, we predict that a combination of drugs enhancing anti-tumor immune response with drugs diminishing tumor aggressiveness will be the most efficient. This is confirmed by the clinical benefit obtained when chemotherapies reducing the tumor cell division rate a are combined with immunotherapies increasing A and R , [50]. The parameter A which governs the efficacy of the immune system to eliminate tumor cells, is the most influential. This finding correlates with the observation that “hot” tumors infiltrated with immune cells have better prognostic than “cold” tumors [51] and that the immune cells with the strongest positive impact on patient’s survival are the cytotoxic CD8⁺ T cells [52]. It is also in line with the success of immune checkpoint inhibitors which revert immune tolerance triggered by chronic activation and upregulation of exhaustion markers on effector T and NK cells, thus not only increasing the parameter A but also R [53]. The leading role of the parameter A is also validated by experimental studies and clinical trials, including adoptive transfer of CAR-T and CAR-NK cells engineered to attack cancer cells, immunomodulating antibody therapies or cancer vaccines which boost the anti-tumor immune response [50, 54, 55]. Finally, our finding that the parameter γ is highly influential is validated by the administration of cytokines that stimulate and increase effector T and NK cell survival which are efficient at controlling tumor growth [55]. Thus, altogether, these experimental and clinical data validate the numerical method.

Interestingly, besides the dominant role of the parameter A , only two additional parameters related to immune cells R , γ seems to have an influence on the tumor mass at equilibrium. These data predict that to enhance the immune response, it is more efficient to increase the rate of influx and conversion of naive immune cells into effector cells (parameter R) or to increase the lifespan of immune effectors (parameter γ) than to increase chemotaxis as a whole (parameters χ , A_σ , \mathcal{K}). The lack of influence of chemotaxis emphasizes that the localization of immune cells within tumors is necessary but not sufficient. Indeed, the leading influence of the parameters A , R , γ stresses the importance of having functional immune cells infiltrating tumors. Overcoming immune suppression is therefore highly relevant in therapeutic strategies.

In conclusion, clinical trials have been undertaken quite often on assumptions from acquired knowledge on tumor development and immune responses to cancer cells, but without tools to help the decision-making. The numerical methods developed here provide valuable hints for the design and the optimization of anti-tumor therapies. The approach is validated by clinical evidence obtained so far. By adapting the range of the parameters to the biological values, one can more precisely adapt the therapeutic strategies to specific types of tumors. We thus conclude that mathematical modelling combined with numerical validation provide valuable information that could contribute to better stratify the patients eligible for treatments and consequently save time and lives. In addition, it could also help to decrease the burden of treatment cost providing hints on optimized therapeutic strategies.

Materials and Methods

Mice FVB/N wild-type (WT) mice (Charles River Laboratories, St Germain Nuelles, France) were bred and housed in specific-pathogen-free conditions. Experiments were performed using 6-7 week-old female FVB/N, in compliance with institutional guidelines and have been approved by the regional committee for animal experimentation (reference MESR 2016112515599520; CIEPAL, Nice Côte d’Azur, France).

In vivo tumor growth mSCC38 tumor cell line was established from DMBA/PMA induced sSCCs and maintained in DMEM (Gibco-ThermoFisher Scientific, Courtaboeuf, France) supplemented with 10% heat-inactivated fetal bovine serum (FBS) (GE Healthcare, Chicago, Illinois, USA) penicillin (100 U/ml) and streptomycin (100 $\mu g/ml$) (Gibco-ThermoFisher Scientific, Courtaboeuf, France). 5×10^5 mSCC38 were intradermally injected in anesthetized mice after dorsal skin shaving. Tumor volume was measured manually using a ruler and calculated according to the ellipsoid formula: Volume=Length (mm) \times Width (mm) \times Height (mm) $\times \pi/6$.

Tissue preparation and cell count mSCC38 were excised and enzymatically treated twice with collagenase IV (1 mg/ml) (Sigma-Aldrich, St Quentin Fallavier, France), and DNase I (0.2 mg/ml) (Roche Diagnostic, Meylan, France) for 20 minutes at 37° C. Total cell count was obtained on a Casy cell counter (Ovni Life Science, Bremen, Germany). Immune cell count was determined from flow cytometry analysis. Briefly, cell suspensions were incubated with anti-CD16/32 (2.4G2) to block Fc receptors and stained with anti-CD45 (30-F11)-BV510 antibody and the 7-Aminoactinomycin D (7-AAD) to identify live immune cells (BD Biosciences, Le Pont de Claix, France). Samples were acquired on a BD LSR Fortessa and analyzed with DIVA V8

and FlowJo V10 software (BD Biosciences, Le Pont de Claix, France).

Mathematical and statistical analysis Computations were realized in Python and we made use of dedicated libraries, in particular the gmsh library for the computational domain mesh generation, the packages optimize (for the optimization methods using the Levenberg-Marquard mean square algorithm; similar results have been obtained with the CMA-ES algorithm of the library cma) from the library scipy, the library Pygpc for the generalized Polynomial Chaos approximation [56] and the library Salib for the sensitivity analysis [57].

Authors' Contributions

Conception and design: K. Atsou, V. M. Braud, T. Goudon

Development of methodology: K. Atsou, V. M. Braud, T. Goudon

Acquisition of data (provided animals, acquired and managed patients, provided facilities, etc.): F. Anjuère, V. M. Braud, S. Khou

Analysis and interpretation of data (e.g., statistical analysis, biostatistics, computational analysis): K. Atsou, V. M. Braud, T. Goudon

Writing, review, and/or revision of the manuscript: K. Atsou, F. Anjuère, V. M. Braud, T. Goudon

Study supervision: F. Anjuère, V. M. Braud, T. Goudon

Acknowledgements

The authors acknowledge the support of UCAnCer, an incentive Université Côte d'Azur network, which has permitted and encouraged this collaboration. We thank the IPMC's animal house and Imaging/Flow cytometry core facilities for technical support. This work was supported by the French Government (National Research Agency, ANR) through the "Investments for the Future" programs LABEX SIGNALIFE ANR-11-LABX-0028 and IDEX UCAJedi ANR-15-IDEX-01.

Code availability

Codes are available at the URL <https://github.com/atsoukevin93/tumorgrowth>

Data availability

Numerical data necessary to replicate the results of the paper are available at the URL <https://github.com/atsoukevin93/tumorgrowth>

References

- [1] Dunn, G. P., Bruce, A. T., Ikeda, H., Old, L. J. & Schreiber, R. D. Cancer immunoediting: from immunosurveillance to tumor escape. *Nat. Immunol.* **3**, 991–998 (2002).

- [2] Boon, T., Coulie, P. G., den Eynde, B. J. V. & van der Bruggen, P. Human T-cell responses against melanoma. *Annual Review of Immunology* **24**, 175–208 (2006). URL <https://doi.org/10.1146/annurev.immunol.24.021605.090733>. PMID: 16551247, <https://doi.org/10.1146/annurev.immunol.24.021605.090733>.
- [3] Dranoff, G. Cytokines in cancer pathogenesis and cancer therapy. *Nature Reviews Cancer* **4**, 11–22 (2004).
- [4] Rabinovich, G. A., Gabrilovich, D. & Sotomayor, E. M. Immunosuppressive strategies that are mediated by tumor cells. *Ann. Rev. Immunol.* **25**, 267–296 (2007). URL <https://doi.org/10.1146/annurev.immunol.25.022106.141609>. PMID: 17134371, <https://doi.org/10.1146/annurev.immunol.25.022106.141609>.
- [5] Smyth, M. J., Godfrey, D. I. & Trapani, J. A. A fresh look at tumor immunosurveillance and immunotherapy. *Nat. Immunol.* **2**, 293–299 (2001).
- [6] Whiteside, T. L. Immune suppression in cancer: Effects on immune cells, mechanisms and future therapeutic intervention. *Seminars in Cancer Biology* **16**, 3–15 (2006). URL <http://www.sciencedirect.com/science/article/pii/S1044579X0500060X>. The Inflammation-Cancer Linkage: A Double-Edged Sword?
- [7] Koebel, C. M. *et al.* Adaptive immunity maintains occult cancer in an equilibrium state. *Nature* **450**, 903–908 (2007).
- [8] Atsou, K., Anjuère, F., Braud, V. M. & Goudon, T. A size and space structured model describing interactions of tumor cells with immune cells reveals cancer persistent equilibrium states in tumorigenesis. *J. Theor. Biol.* **490**, 110163 (2020).
- [9] Kirschner, D. E. & Panetta, J. C. Modeling immunotherapy of the tumor-immune interaction. *J. Math. Biol.* **37**, 235–252 (1998).
- [10] Konstorium, A., Vella, A. T., Adler, A. J. & Laubacher, R. C. Addressing current challenges in cancer immunotherapy with mathematical and computational modelling. *J. Royal Soc. Interface* **14**, # 20170150 (2017). 1706.01989.
- [11] Lai, X. *et al.* Modeling combination therapy for breast cancer with BET and immune checkpoint inhibitors. *Proc. Nat. Acad. Sc.* **115**, 5534–5539 (2018).
- [12] de Pillis, L. G., Radunskaya, A. E. & Wiseman, C. L. A validated mathematical model of cell-mediated immune response to tumor growth. *Cancer Res.* **65**, 7950–7958 (2005). URL <http://cancerres.aacrjournals.org/content/65/17/7950>. <http://cancerres.aacrjournals.org/content/65/17/7950.full.pdf>.

- [13] Eftimie, R., Bramson, J. L. & Earn, D. J. D. Interactions between the immune system and cancer: A brief review of non-spatial mathematical models. *Bull. Math. Biol.* **73**, 2–32 (2011). URL <https://doi.org/10.1007/s11538-010-9526-3>.
- [14] Wilkie, K. P. & Hahnfeldt, P. Modeling the dichotomy of the immune response to cancer: Cytotoxic effects and tumor-promoting inflammation. *Bull. Math. Biol.* **79**, 1426–1448 (2017).
- [15] Doumic-Jauffret, M. & Gabriel, P. Eigenelements of a general aggregation-fragmentation model. *Math. Models Methods Appl. Sci.* **20**, 757–783 (2010). URL <https://doi.org/10.1142/S021820251000443X>.
- [16] Khou, S. *et al.* Tumor-associated neutrophils dampen adaptive immunity and promote cutaneous squamous cell carcinoma development. *Cancers* **10-12**, E1860 (2020).
- [17] Farrell, B. E., Daniele, R. P. & Lauffenburger, D. A. Quantitative relationships between single-cell and cell-population model parameters for chemosensory migration responses of alveolar macrophages to C5a. *Cell Motility* **16**, 279–293 (1990). URL <https://onlinelibrary.wiley.com/doi/abs/10.1002/cm.970160407>. <https://onlinelibrary.wiley.com/doi/pdf/10.1002/cm.970160407>.
- [18] Friedman, A. & Hao, W. The role of exosomes in pancreatic cancer microenvironment. *Bull. Math. Biol.* **80**, 1111–1133 (2018). URL <https://doi.org/10.1007/s11538-017-0254-9>.
- [19] Matzavinos, A., Chaplain, M. A. J. & Kuznetsov, V. A. Mathematical modelling of the spatio-temporal response of cytotoxic *T*-lymphocytes to a solid tumour. *Math. Medicine and Biology* **21**, 1–34 (2004).
- [20] Yates, A. & Callard, R. Cell death and the maintenance of immunological memory. *Disc. Cont. Dyn. Syst.-B* **1**, 43–59 (2001).
- [21] Chaplain, M. A., Kuznetsov, V. A., James, Z. H., Davidson, F. & Stepanova, L. A. Spatio-temporal dynamics of the immune system response to cancer. In Horn, M. A., Gieri, S. & Webb, G. F. (eds.) *Mathematical models in medical and health science* (Vanderbilt University Press, 1998). International Conference on Mathematical Models in Medical and Health Sciences.
- [22] Kuznetsov, V. A., Makalkin, I. A., Taylor, M. A. & Perelson, A. S. Nonlinear dynamics of immunogenic tumors: Parameter estimation and global bifurcation analysis. *Bull. Math. Biol.* **56**, 295–321 (1994). URL <https://doi.org/10.1007/BF02460644>.
- [23] Beck, R. J., Slagter, M. & Beltman, J. B. Contact-dependent killing by cytotoxic *T* lymphocytes is insufficient for EL4 tumor regression in vivo. *Cancer Research* **79**, 3406–3416 (2019). URL <https://cancerres.aacrjournals.org/content/79/13/3406>. <https://cancerres.aacrjournals.org/content/79/13/3406.full.pdf>.
- [24] Cazaux, M. *et al.* Single-cell imaging of CAR *T*-cell activity in vivo reveals extensive functional and anatomical heterogeneity. *J. Experimental Medicine* **216**, 1038–1049 (2019).
- [25] Hanson, H. L. *et al.* Eradication of established tumors by *CD8+* *T*-cell adoptive immunotherapy. *Cell Press* **13**, 265–276 (2000).
- [26] Nolz, J. C. & Hill, A. B. Strength in numbers: Visualizing CTL-mediated killing in vivo. *Immunity* **44**, 207–208 (2016). URL <http://www.sciencedirect.com/science/article/pii/S1074761316300139>.
- [27] Kwok, C. S., Cole, S. E. & Liao, S.-K. Uptake kinetics of monoclonal antibodies by human malignant melanoma multicell spheroids. *Cancer Res.* **48**, 1856–1863 (1988). URL <https://cancerres.aacrjournals.org/content/48/7/1856>. <https://cancerres.aacrjournals.org/content/48/7/1856.full.pdf>.
- [28] Cairns, C. M. *et al.* Lymphotactin Expression by Engineered Myeloma Cells Drives Tumor Regression: Mediation by *CD4+* and *CD8+* *T*-Cells and Neutrophils Expressing *XCR1* Receptor. *J. Immun.* **167**, 57–65 (2001).
- [29] Michel, P. Existence of a solution to the cell division eigenproblem. *Models Math. Meth. App. Sci.* **16**, 1125–1153 (2006).
- [30] Michel, P., Mischler, S. & Perthame, B. General relative entropy inequality: an illustration on growth models. *J. Math. Pures et Appl.* **84**, 1235–1260 (2005).
- [31] Perthame, B. & Ryzhik, L. Exponential decay for the fragmentation or cell-division equation. *J. Differ. Eq.* **210**, 155–177 (2005).
- [32] Moré, J. J. The Levenberg-Marquardt algorithm: Implementation and theory. In Watson, G. A. (ed.) *Numerical Analysis*, 105–116 (Springer Berlin Heidelberg, Berlin, Heidelberg, 1978).
- [33] Ramadasan, D., Chevaldonné, M. & Chateau, T. LMA: A generic and efficient implementation of the Levenberg-Marquardt algorithm. *Software: Practice and Experience* **47**, 1707–1727 (2017).
- [34] Baccelli, F., McDonald, D. & Reynier, J. A mean field model for multiple TCP connections through a buffer

- 858 implementing RED. *Performance Evaluation* **49**, 77–97
859 (2002).
- 860 [35] Shashni, B. *et al.* Size-based differentiation of cancer and
861 normal cells by a particle size analyzer assisted by a cell-
862 recognition pc software. *Biological and Pharmaceutical*
863 *Bulletin* **41**, 487–503 (2018).
- 864 [36] Faget, J. *et al.* Neutrophils and snail orchestrate the
865 establishment of a pro-tumor microenvironment in lung
866 cancer. *Cell Report* **21**, 3190–3204 (2017).
- 867 [37] Li, C.-Y. *et al.* Initial stages of tumor cell-induced
868 angiogenesis: evaluation via skin window chambers in
869 rodent models. *J. Nat. Cancer Institute* **92**, 143–
870 147 (2000). URL [https://doi.org/10.1093/jnci/92.2.](https://doi.org/10.1093/jnci/92.2.143)
871 [https://academic.oup.com/jnci/article-pdf/92/2/](https://academic.oup.com/jnci/article-pdf/92/2/143/9996237/143.pdf)
872 [143/9996237/143.pdf](https://academic.oup.com/jnci/article-pdf/92/2/143/9996237/143.pdf).
- 873 [38] Goudon, T. *Mathematics for Modeling and Scientific*
874 *Computing*. Mathematics and Statistics (Wiley-ISTE,
875 2016).
- 876 [39] Chatelin, F. Convergence of approximation methods to
877 compute eigenlements of linear operations. *SIAM J.*
878 *Numer. Anal.* **10**, 939–948 (1973).
- 879 [40] Chatelin, F. The spectral approximation of linear oper-
880 ators with applications to the computation of eigenele-
881 ments of differential and integral operators. *SIAM Rev.*
882 **23**, 495–522 (1981).
- 883 [41] Erdi, Y. E. Limits of tumor detectability in nuclear
884 medicine and PET. *Molecular imaging and radionuclide*
885 *therapy* **21**, 23–28 (2012).
- 886 [42] Harenberg, D., Marelli, S., Sudret, B. & Winschel, V.
887 Uncertainty quantification and global sensitivity analysis
888 for economic models. *Quantitative Economics* **10**, 1–41
889 (2019).
- 890 [43] Saltelli, A. Sensitivity analysis of model output. An in-
891 vestigation of new techniques. *Computational Statistics*
892 *and Data Analysis* **15**, 211–238 (1993).
- 893 [44] Sobol’, I. Sensitivity estimates for nonlinear mathemat-
894 ical models. *Math. Modell. Comput.* **1**, 407–414 (1993).
- 895 [45] Crestaux, T., Le Maître, O. & Martinez, J.-M. Polyno-
896 mial chaos expansion for sensitivity analysis. *Reliability*
897 *Engineering and System Safety* **94**, 1161–1172 (2009).
- 898 [46] Sudret, B. Global sensitivity analysis using polynomial
899 chaos expansions. *Reliability Engineering and System*
900 *Safety* **93**, 964–979 (2008).
- 901 [47] Ernst, O. G., Mugler, A., Starkloff, H. J. & Ullmann,
902 E. On the convergence of generalized polynomial chaos
903 expansions. *ESAIM: Mathematical Modelling and Nu-*
904 *merical Analysis* **46**, 317–339 (2012).
- 905 [48] Le Gratiot, L., Marelli, S. & Sudret, B. Metamodel-
906 based sensitivity analysis: Polynomial chaos expansions
907 and gaussian processes. In Ghanem, R., Higdon, D.
908 & Owhadi, H. (eds.) *Handbook of Uncertainty Quan-*
909 *tification*, 1289–1325 (Springer International Publishing,
910 Cham, 2017). URL [https://doi.org/10.1007/978-3-319-](https://doi.org/10.1007/978-3-319-12385-1_38)
911 [12385-1_38](https://doi.org/10.1007/978-3-319-12385-1_38).
- 912 [49] Saltelli, A. Making best use of model evaluations to
913 compute sensitivity indices. *Computer Physics Comm.*
914 **145**, 280 – 297 (2002). URL [http://www.sciencedirect.](http://www.sciencedirect.com/science/article/pii/S0010465502002801)
915 [com/science/article/pii/S0010465502002801](http://www.sciencedirect.com/science/article/pii/S0010465502002801).
- 916 [50] Bailly, C., Thuru, X. & Quesnel, B. Combined cytotoxic
917 chemotherapy and immunotherapy of cancer: modern
918 times. *NAR Cancer* **2**, 1–20 (2020).
- 919 [51] Galon, J. & Bruni, D. Approaches to treat immune hot,
920 altered and cold tumours with combination immunother-
921 apies. *Nature Rev. Drug Discovery* **18**, 197–218 (2019).
- 922 [52] Galon, J. *et al.* Type, density, and location of immune
923 cells within human colorectal tumors predict clinical out-
924 come. *Science* **313**, 1960–1964 (2006).
- 925 [53] Sharma, P. & Allison, J. The future of immune check-
926 point therapy. *Science* **348**, 56–61 (2015).
- 927 [54] Champiat, S. *et al.* Intratumoral immunotherapy: from
928 trial design to clinical practice. *Clin. Cancer Res.* (2020).
- 929 [55] Shekarian, T., Valsesia-Wittmann, S., Caux, C. & Mara-
930 belle, A. Paradigm shift in oncology: targeting the im-
931 mune system rather than cancer cells. *Mutagenesis* **30**,
932 205–211 (2015).
- 933 [56] Weise, K., Poßner, L., Müller, E., Gast, R. & Knösche,
934 T. R. Pygpc: A sensitivity and uncertainty analysis tool-
935 box for Python. *SoftwareX* **11**, 100450 (2020). URL
936 <https://doi.org/10.1016/j.softx.2020.100450>.
- 937 [57] Herman, J. & Usher, W. SALib: An open-source
938 Python library for sensitivity analysis. *The Journal*
939 *of Open Source Software* **2**, joss00097 (2017). URL
940 <https://doi.org/10.21105/joss.00097>.
- 941 [58] Perthame, B. *Transport equations in biology*. Frontiers
942 in Math. (Birkhauser, 2007).
- 943 [59] Krein, M. & Rutman, M. Linear operator leaving in-
944 variant a cone in a Banach space. *Amer. Math. Soc.*
945 *Translation* **10**, 199–325 (1962).
- 946 [60] Serre, D. *Matrices: theory and applications*, vol. 216 of
947 *Graduate Texts in Math.* (Springer, 2002).
- 948 [61] Homma, T. & Saltelli, A. Importance measures in
949 global sensitivity analysis of nonlinear models. *Relia-*
950 *bility Engineering & System Safety* **52**, 1 – 17 (1996).
951 URL [http://www.sciencedirect.com/science/article/pii/](http://www.sciencedirect.com/science/article/pii/S0951832096000026)
952 [0951832096000026](http://www.sciencedirect.com/science/article/pii/S0951832096000026).

Supplementary material

Cell division operator

The binary division operator (2) is a particular case, and for applications it is relevant to deal with more general expressions. Namely, we have

$$Q(n)(t, z) = -a(z)n(t, z) + \int_z^\infty a(z')k(z|z')n(t, z') dz'. \quad (15)$$

In (15), $a(z')$ is the frequency of division of cells having size z' , and $k(z|z')$ gives the size-distribution that results from the division of a tumor cell with size z' . What is crucial for modeling purposes is the requirement

$$\int_0^z z'k(z'|z) dz' = z,$$

which is related to the principle that cell-division does not change the total mass

$$\int_0^\infty zQ(n) dz = 0.$$

We refer the reader to [15] for examples of such cell-division operators.

Equilibrium states

The equilibrium state is characterized by means of an eigenproblem: we look for $\lambda > 0$ and a non negative function $z \geq 0 \mapsto N(z)$ satisfying (10). The analysis of the existence-uniqueness of the eigenpair (λ, N) can be found in [29], the textbook [58, Theorem 4.6], and, for extension to cases with non constant growth rate V , in [15].

Coming back to the coupled model, we infer that the equilibrium phase corresponds to the situation where the death rate precisely counterbalances the natural exponential growth of the tumor cell population. Let Φ be the solution of

$$-\Delta_x \Phi = \sigma - \frac{1}{|\Omega|} \int_\Omega \sigma(y) dy,$$

endowed with the homogeneous Neumann boundary condition. Note that this quantity is a priori defined; it does not depend on the coupling between tumor cells and immune cells. In a computational perspective, it can thus be pre-computed once for all. The equilibrium mass μ_1 is implicitly defined by the fact that the solution of the stationary equation (11) satisfies the constraint (12). This implicit definition is clarified by the following statement, see [8].

Theorem .1 *Let $g : [0, \infty) \rightarrow [0, \infty]$ be a non decreasing function such that $g(0) = 0$, and let $x \mapsto pS(x) \in L^2(\Omega)$ be a non negative function. If $\ell > 0$ is small enough, there exists a unique $\bar{\mu}_1(\ell) > 0$ such that $C_{\bar{\mu}_1(\ell)}$, solution of the stationary equation (11) satisfies $\int_\Omega \delta C dx = \ell$.*

Theorem .1 requires a smallness assumption; for (2) with a constant division rate a , this is a smallness assumption on a . Numerical experiments have shown different large time behaviors for the evolution problem (1a)-(1e):

- when the source term S is space-homogeneous, the expected behavior seems to be very robust. The immune cell concentration tends to fulfill the constraint (12) as time becomes large, and the size repartition of tumor cells tends to the eigenfunction N . The total mass μ_1 tends to a constant; however the asymptotic value cannot be predicted easily. We again refer the reader to Fig. 2 for an illustration of these facts.
- When S has spacial variations, the asymptotic behavior seems to be much more sensitive to the smallness condition. On short time scale of simulations, we observe alternance of growth and remission phases, and the damping to the equilibrium could be very slow.

These observations bring out the complementary roles of different type of cytotoxic cells [36]. The NK cells could be seen as a space-homogenous source of immune cells, immediately available to fight against the tumor, at the early stage of tumor growth. In contrast, T -cells need an efficient priming which occurs in the draining lymph nodes, and their sources is therefore non-homogeneously distributed. Eventually, NK and $CD8^+$ T -cells cooperate to the anti-tumor immune response.

Computation of the eigen-elements of the growth-fragmentation equation

It is important to bear in mind the main arguments of the proof of the existence-uniqueness of the eigenpair (λ, N) for the growth-fragmentation equation. Namely, for Λ large enough we consider the *shifted* operator

$$\mathcal{T}_\Lambda N = \Lambda N + \partial_z(VN) + aN - \int_z^\infty a(z')k(z|z')N(z') dz'.$$

Then, we check that the operator \mathcal{S}_Λ which associates to a function f the solution n of $\mathcal{T}_\Lambda n = f$ fulfills the requirements of the Krein-Rutman theorem (roughly speaking, positivity and compactness), see [59]. Accordingly, the quantity of interest λ is related to the leading eigenvalue of \mathcal{S}_Λ . In fact, this reasoning should be applied to a somehow truncated and regularized version of the operator, and the conclusion needs further compactness arguments; nevertheless this is the essence of the proof. In terms of numerical method, this suggests to appeal to the inverse power algorithm, applied to a discretized version of the equation. However, we need to define appropriately the shift parameter Λ . As far as the continuous problem is considered, Λ can be estimated by the parameters of the model [15], but it is critical for practical issues to check whether or not this condition is impacted by the discretization procedure. This information will be used to apply the

inverse power method to the discretized and shifted version of the problem.

Analysis of the discrete problem

The computational domain for the size variable is the interval $[0, R]$ where R is chosen large enough: due to the division processes, we expect that the support of the solution remains essentially on a bounded interval, and the cut-off should not perturb too much the solution. In what follows, the size step $h = z_{i+1} - z_i$ is assumed to be constant. The discrete unknowns N_i , with $i \in \{1, \dots, I\}$ and $h = R/I$, are intended to approximate $N(z_i)$ where $z_i = ih$. The integral that defines the gain term of the division operator is approximated by a simple quadrature rule. For the operator (2) the kernel involves Dirac masses which can be approached by peaked Gaussian. We introduce the operator $\mathcal{T}_\Lambda^h : \mathbb{R}^I \rightarrow \mathbb{R}^I$ defined by

$$\begin{cases} (\mathcal{T}_\Lambda^h N)_i = F_i - F_{i-1} + h(\Lambda + a_i)N_i \\ \quad - h^2 \sum_{j=i}^I a(z_j)k(z_i|z_j)N_j, \\ N_1 = 0 \end{cases} \quad (16)$$

where $F_i = V_{i+1/2}N_i$ represents the convective numerical flux on the grid point $z_{i+1/2} = (i+1/2)h$, $i \in \{1, \dots, I\}$. This definition takes into account that the growth rate is non negative, and applies the upwinding principles. Note that the step size h should be small enough to capture the division of small cells, if any. The following statement provides the a priori estimate which allows us to determine the shift for the discrete problem.

Theorem .2 *We suppose that*

- i) $z \mapsto V(z)$ is a continuous function which lies in L^∞ and it is bounded from below by a positive constant,
- ii) $h \sum_{j=1}^I a(z_j)k(z_i|z_j)$ remains bounded uniformly with respect to h ,
- iii) for any $i \in \{1, \dots, I-1\}$, there exists $j \in \{i+1, \dots, I\}$ such that $a(z_j)k(z_i|z_j) > 0$,
- iv) there exists $Z_0 \in (0, \infty)$ such that, setting $\bar{N}(z) = h \sum_{j=2}^I k(z_j|z)$, we have $a(z)(\bar{N}(z) - 1) \geq \nu_0 > 0$ for any $z \geq Z_0$.

Let

$$\Lambda > \frac{\|V\|_{L^\infty}}{\min_{j \in \{1, \dots, I\}} |V_{j+1/2}|} \max_{k \in \{1, \dots, I\}} \left(h \sum_{j=k}^I a_j k(z_k|z_j) \right) - \min_{j \in \{1, \dots, I\}} |a_j|, \quad (17)$$

and we suppose that $R > Z_0$ is large enough. Then, \mathcal{T}_Λ^h is invertible and there exists a pair $\mu > 0$, $N \in \mathbb{R}^I$ with positive components, such that $\text{Ker}((\mathcal{T}_\Lambda^h)^{-1} - \mu) = \text{Span}\{N\}$. Moreover $\lambda = \Lambda - \frac{1}{\mu} > 0$.

Note that the sum that defines $\bar{N}(z)$ is actually reduced over the indices such that $jh \leq z$; this quantity is interpreted as the expected number of cells produced from the division of a cell with size z so that the forth assumption is quite natural.

Proof. Let $f \in \mathbb{R}^I$. We consider the equation

$$\mathcal{T}_\Lambda^h N = f.$$

We denote $N = \mathcal{S}_\Lambda^h f$ the solution. We are going to show that \mathcal{S}_Λ^h is well defined and satisfies the assumptions of the Perron-Frobenius theorem, see e. g. [38, Theorem 1.37 & Corollary 1.39] or [60, Chapter 5].

It is convenient to introduce the change of unknown $U_i = N_i V_{i+1/2}$, $\forall i \in \{1, \dots, I\}$. The problem recasts as

$$\begin{cases} (\widetilde{\mathcal{T}}_\Lambda^h U)_i = h \frac{f_i}{V_{i+1/2}}, \text{ with} \\ (\widetilde{\mathcal{T}}_\Lambda^h U)_i = U_i - U_{i-1} + h \frac{\Lambda + a_i}{V_{i+1/2}} U_i \\ \quad - h^2 \sum_{j=i}^I \frac{a_j}{V_{j+1/2}} k(z_i|z_j) U_j, \\ U_1 = 0. \end{cases} \quad (18)$$

The solution is interpreted as the fixed point of the mapping

$$\xi \longmapsto U = A^h \xi$$

where U is given by $U_1 = 0$ and

$$U_i = U_{i-1} + h^2 \sum_{j=i}^I \frac{a_j}{V_{j+1/2}} k(z_i|z_j) \xi_j + h \frac{f_i}{V_{i+1/2}}.$$

We are going to show that A^h is a contraction: $\|A^h \xi\|_{\ell^\infty} \leq k \|\xi\|_{\ell^\infty}$ for some $k < 1$. Multiplying (18) by $\text{sign}(U_i)$, we obtain

$$\begin{aligned} \left(1 + h \frac{\Lambda + a_i}{V_i}\right) \text{sign}(U_i) U_i &= \left(1 + h \frac{\Lambda + a_i}{V_i}\right) |U_i| \\ &= \text{sign}(U_i) U_{i-1} + h^2 \sum_{j=i}^I \frac{a_j}{V_{j+1/2}} k(z_i|z_j) \text{sign}(U_i) \xi_j \\ &\leq |U_{i-1}| + h^2 \sum_{j=i}^I \frac{a_j}{V_{j+1/2}} k(z_i|z_j) |\xi_j|. \end{aligned}$$

We multiply this by the weight $\prod_{l=1}^{i-1} [1 + h \frac{\Lambda + a_l}{V_{l+1/2}}]$, where all factors are ≥ 1 . We get

$$\begin{aligned} |U_i| \prod_{l=1}^i \left[1 + h \frac{\Lambda + a_l}{V_{l+1/2}}\right] \\ \leq |U_{i-1}| \prod_{l=1}^{i-1} \left[1 + h \frac{\Lambda + a_l}{V_{l+1/2}}\right] \\ + h^2 \prod_{l=1}^i \left[1 + h \frac{\Lambda + a_l}{V_{l+1/2}}\right] \sum_{j=i}^I \frac{a_j}{V_{j+1/2}} k(z_i|z_j) |\xi_j|. \end{aligned}$$

1087 Then, summing over $i \in \{2, \dots, m\}$ yields

$$\begin{aligned} |U_m| & \prod_{l=1}^m \left[1 + h \frac{\Lambda + a_l}{V_{l+1/2}} \right] \\ & \leq |U_1| \left[1 + h \frac{\Lambda + a_1}{V_{3/2}} \right] \\ & \quad + h^2 \sum_{i=2}^m \prod_{l=1}^i \left[1 + h \frac{\Lambda + a_l}{V_{l+1/2}} \right] \sum_{j=i}^I \frac{a_j}{V_{j+1/2}} k(z_i|z_j) |\xi_j| \end{aligned}$$

1088 where actually $U_1 = 0$. It follows that

$$\begin{aligned} |U_m| & \leq h^2 \sum_{i=2}^m \prod_{l=i}^m \left[1 + h \frac{\Lambda + a_l}{V_{l+1/2}} \right]^{-1} \sum_{j=i}^I \frac{a_j}{V_{j+1/2}} k(z_i|z_j) |\xi_j| \\ & \leq \frac{h^2 \|\xi\|_{\ell^\infty}}{\min_{j \in \{1, \dots, I\}} V_{j+1/2}} \sum_{i=2}^m \prod_{l=i}^m \left[1 + h \frac{\Lambda + a_l}{V_{l+1/2}} \right]^{-1} \sum_{j=i}^I a_j k(z_i|z_j) \\ & \leq \frac{h^2 \|\xi\|_{\ell^\infty}}{\min_{j \in \{1, \dots, I\}} V_{j+1/2}} \left\| \sum_{j=i}^I a_j k(z_i|z_j) \right\|_{\ell^\infty} \\ & \quad \sum_{i=2}^m \left[1 + h \frac{\Lambda + \min_{l \in \{1, \dots, I\}} a_l}{\|V\|_{L^\infty}} \right]^{i-m+1} \\ & \leq \frac{h \|\xi\|_{\ell^\infty}}{\min_{j \in \{1, \dots, I\}} V_{j+1/2}} \left\| \sum_{j=i}^I a_j k(z_i|z_j) \right\|_{\ell^\infty} \\ & \quad \left[\frac{\Lambda + \min_{l \in \{1, \dots, I\}} a_l}{\|V\|_{L^\infty}} \right]^{-1}. \end{aligned}$$

1089 Therefore, A^h is a contraction provided (17) holds. This estimate is similar to the condition obtained for the continuous problem, see [15, Proof of Theorem 2, Appendix B]; the discretization does not introduce further constraints.

1093 We are now going to show that \mathcal{F}_Λ^h is a M -matrix when (17) holds. Let $f \in \mathbb{R}^I \setminus \{0\}$ with non negative components. Let $U \in \mathbb{R}^I$ satisfy $(\mathcal{F}_\Lambda^h U)_i = h \frac{f_i}{V_{i+1/2}}$. Let i_0 be the index such that $U_{i_0} = \min \{U_i, i \in \{2, \dots, I\}\}$. We have

$$\begin{aligned} & U_{i_0} \left(1 + h \frac{\Lambda + a_{i_0}}{V_{i_0+1/2}} \right) \\ & = U_{i_0-1} + h^2 \sum_{j=i_0}^I \frac{a_j}{V_{j+1/2}} k(z_{i_0}|z_j) U_j + h \frac{f_{i_0}}{V_{i_0+1/2}} \\ & \geq U_{i_0} \left(1 + h^2 \sum_{j=i_0}^I \frac{a_j}{V_{j+1/2}} k(z_{i_0}|z_j) \right) + h \frac{f_{i_0}}{V_{i_0+1/2}}. \end{aligned} \quad (19)$$

1097 Since $f_{i_0} \geq 0$, we get

$$U_{i_0} \underbrace{\left(\frac{\Lambda + a_{i_0}}{V_{i_0+1/2}} - h \sum_{j=i_0}^I \frac{a_j}{V_{j+1/2}} k(z_{i_0}|z_j) \right)}_{>0 \text{ by (17)}} \geq 0,$$

1098 which tells us that $U_{i_0} \geq 0$. Suppose $U_{i_0} = 0$ for some $i_0 > 1$. Coming back to (19), we deduce that U_{i_0-1} vanishes too, 1099 and so on and so forth, we obtain $U_1 = \dots = U_{i_0} = 0$. Finally, we use the irreducibility assumption iii): we can 1100 find $j_0 > i_0$ such that $\frac{a_{j_0}}{V_{j_0+1/2}} k(z_{i_0}|z_{j_0}) > 0$ and (19) implies 1101 $\frac{a_{j_0}}{V_{j_0+1/2}} k(z_{i_0}|z_{j_0}) U_{j_0} = 0$, so that $U_{j_0} = 0$. We deduce that 1102 1103

1104 $U = 0$, which contradicts $f \neq 0$. Therefore the components 1105 of U are positive, but U_1 .

We conclude by applying the Perron-Frobenius theorem to $(\mathcal{F}_\Lambda^h)^{-1}$, [60, Chapter 5]. It remains to prove that $\lambda = \Lambda - \frac{1}{\mu}$ is positive, with μ the spectral radius of $(\mathcal{F}_\Lambda^h)^{-1}$. To this end, we make use of assumption iv). We set $Z_0 = i_0 h$. We argue by contradiction, supposing that $\lambda = \Lambda - 1/\mu < 0$. We consider the eigenvector with positive components and normalized by the condition $h \sum_{i=1}^I U_i = 1$. We have

$$\begin{aligned} (\mathcal{F}_0^h U)_i & = U_i - U_{i-1} + \frac{a_i}{V_{i+1/2}} h U_i \\ & \quad - h^2 \sum_{j=i}^I \frac{a_j}{V_{j+1/2}} k(z_i|z_j) U_j = -\lambda U_i \geq 0. \end{aligned}$$

It follows that, for $m \geq i_0$,

$$\begin{aligned} U_m & \geq -h \sum_{i=2}^m \frac{a_i}{V_{i+1/2}} U_i + h^2 \sum_{i=2}^m \sum_{j=i}^I \frac{a_j}{V_{j+1/2}} k(z_i|z_j) U_j \\ & \geq -h \sum_{i=2}^m \frac{a_i}{V_{i+1/2}} U_i + h \sum_{j=2}^m \left(h \sum_{i=2}^j k(z_i|z_j) \right) \frac{a_j}{V_{j+1/2}} U_j \\ & \geq -h \sum_{i=2}^m \frac{a_i}{V_{i+1/2}} U_i + h \sum_{j=2}^m \bar{\mathcal{N}}(z_j) \frac{a_j}{V_{j+1/2}} U_j \\ & \geq h \sum_{i=2}^m (\bar{\mathcal{N}}(z_i) - 1) \frac{a_i}{V_{i+1/2}} U_i \\ & \geq h \sum_{i=i_0}^m (\bar{\mathcal{N}}(z_i) - 1) \frac{a_i}{V_{i+1/2}} U_i \geq \frac{\nu_0}{\|V\|_{L^\infty}} h \sum_{i=i_0}^m U_i. \end{aligned}$$

1106 It implies

$$1 = h \sum_{m=1}^I U_m \geq h \sum_{m=i_0}^I U_m \geq h(I - i_0) \frac{\nu_0}{\|V\|_{L^\infty}} h \sum_{i=i_0}^m U_i.$$

1107 We arrive at

$$1 \geq (R - Z_0) \frac{\nu_0}{\|V\|_{L^\infty}},$$

1108 a contradiction when R is chosen large enough (but how large 1109 R should be does not depend on h). Therefore, we conclude 1110 that $\lambda > 0$. ■

1111 Numerical approximation of (λ, N)

1112 We compute (an approximation of) the eigenpair (λ, N) by 1113 using the inverse power method which finds the eigenvalue of 1114 $(\mathcal{F}_\Lambda^h)^{-1}$ with largest modulus:

- 1115 • We pick Λ verifying (17).
- 1116 • We compute once for all the LU decomposition of the matrix \mathcal{F}_Λ^h .
- 1117 • We choose a threshold $0 < \epsilon \ll 1$.
- 1118 • We start from a random vector $N^{(0)}$ and we construct the iterations

$$- LUq^{(k+1)} = N^{(k)},$$

$$- N^{(k+1)} = \frac{q^{(k+1)}}{\|q^{(k+1)}\|}$$

until the relative error $\frac{\|N^{(k+1)} - N^{(k)}\|}{\|N^{(k)}\|} \leq \epsilon$ is small enough.

Then, given the last iterate $N^{(K)}$, we set $LUq = N^{(K)}$, $\tilde{\mu} = \frac{q \cdot N^{(K)}}{N^{(K)} \cdot N^{(K)}}$, and $\tilde{\lambda} = \Lambda - 1/\tilde{\mu}$.

This approach relies on the ability to approximate correctly the eigenpair of the growth-fragmentation operator. In particular, it is important to preserve the algebraic multiplicity. This issue is quite subtle and it is known that the pointwise convergence of the operator is not enough to guarantee the convergence of the eigenelements and the consistency of the invariant subspaces, see [39] for relevant examples. This question has been thoroughly investigated in [39, 40] which introduced a suitable notion of stability. It turns out that one needs a uniform convergence of the operators. Namely, here, we should check that $\|(\mathcal{T}_\Lambda^I)^{-1} - (\mathcal{T}_\Lambda)^{-1}\| \rightarrow 0$ as $I \rightarrow \infty$. In the present framework, a difficulty relies on the fact that the size variable lies in an unbounded domain, which prevents for using usual compactness arguments. For this reason, we introduce a truncated version of the problem, which has also to be suitably regularized. Let us denote by $\mathcal{T}_\Lambda^{R,\epsilon}$ the corresponding operator, where ϵ represents the regularization parameter. This truncated and regularized operator appeared already in [15]. Indeed, we know from [15] that $\|\mathcal{T}_\Lambda^{R,\epsilon} - \mathcal{T}_\Lambda\| \rightarrow 0$ as $R \rightarrow \infty$ and $\epsilon \rightarrow 0$, hence, this implies that $\|(\mathcal{T}_\Lambda^{R,\epsilon})^{-1} - (\mathcal{T}_\Lambda)^{-1}\| \rightarrow 0$ as $R \rightarrow \infty$ and $\epsilon \rightarrow 0$ by continuity of the map $\Pi : \mathcal{T}_\Lambda \mapsto (\mathcal{T}_\Lambda)^{-1}$. Moreover, $(\mathcal{T}_\Lambda^{R,\epsilon})^{-1}$ is well-defined, continuous and compact, see [15, Appendix. B]. The discrete operators $(\mathcal{T}_\Lambda^I)^{-1}$ converge pointwise to $(\mathcal{T}_\Lambda^{R,\epsilon})^{-1}$, and the compactness of $(\mathcal{T}_\Lambda^{R,\epsilon})^{-1}$ ensures that the discrete operator converges uniformly to $(\mathcal{T}_\Lambda^{R,\epsilon})^{-1}$, for $0 < R < \epsilon$ and $0 < \epsilon < 1$ fixed (see [40] for more details on this fact). Following [40], we deduce that the numerical eigenelements (λ^I, N^I) converges to $(\lambda^{R,\epsilon}, N^{R,\epsilon})$, the eigenelements of $(\mathcal{T}_\Lambda^{R,\epsilon})^{-1}$, while preserving their algebraic multiplicity. Finally the uniform convergence $\|(\mathcal{T}_\Lambda^{R,\epsilon})^{-1} - (\mathcal{T}_\Lambda)^{-1}\| \rightarrow 0$ as $R \rightarrow \infty$ and $\epsilon \rightarrow 0$ ensures the convergence of $(\lambda^{R,\epsilon}, N^{R,\epsilon})$ to (λ, N) , [15].

Numerical results

For some specific fragmentation kernels and growth rates, the eigenpair (λ, N) is explicitly known, see [15]. We can use these formula to check that the algorithm is able to find the expected values and profiles. To this end, we introduce the relative errors

$$E_\lambda^h = \frac{|\lambda - \tilde{\lambda}|}{\tilde{\lambda}} \quad \text{and} \quad E_V^h = h \sum_{i=1}^I |N_i^{(K)} - N(ih)|$$

where $N^{(K)}$ and N are both normalized by $h \sum_{i=1}^I N_i^{(K)} = h \sum_{i=1}^I N(ih) = 1$.

Mitosis fragmentation kernel. We start with the binary division kernel:

$$k(z|z') = \delta_{z'=2z}. \quad (20)$$

The associated division operator is described by (2). We assume that a and V are constant. In this specific case the eigenpair is given by

$$\lambda = a, \quad N(z) = \bar{N} \sum_{n=0}^{\infty} (-1)^n \alpha_n \exp\left(-2^{n+1} \frac{a}{V} z\right), \quad (21)$$

with $\bar{N} > 0$ an appropriate normalizing constant and $(\alpha_n)_{n \in \mathbb{N}}$ is the sequence defined by the recursion

$$\alpha_0 = 1, \quad \alpha_n = \frac{2}{2^n - 1} \alpha_{n-1}.$$

In practice we shall use a truncated version of the series that defines N . For the numerical tests, we use the parameters collected in Table 3

a	V	R	ϵ
4	0.6	5	10^{-6}

Table 3. Data for the numerical tests: binary division kernel

Number of cells	E_λ	E_V
1000	3.73×10^{-5}	3.83×10^{-2}
2000	5.68×10^{-8}	1.93×10^{-2}
4000	6.77×10^{-7}	9.69×10^{-3}
8000	6.84×10^{-7}	4.85×10^{-3}

Table 4. Binary division kernel: errors for several number of grid points

With this threshold ϵ , the approached eigenpair is reached in 43 iterations, independently of the size step. Fig. 7 represents the evolution of the error E_V^h as a function of h in a log-log scale: $N^{(K)}$ approaches N at order 1. The rate improves when using a quadrature rule with a better accuracy. For this test, the approximation of the eigenvalue is already accurate with a coarse grid; it is simply driven by the threshold ϵ and E_L^h does not significantly change with h .

Uniform fragmentation. The uniform fragmentation kernel is defined by:

$$k(z|z') = \frac{1}{z'} \mathbb{1}_{0 \leq z \leq z'}.$$

We apply the algorithm for the following two cases:

1. $V(z) = V_0$ and $a(z) = a_0 z$. We have $\lambda = \sqrt{a_0 V_0}$ and

$$N(z) = 2\sqrt{\frac{a_0}{V_0}} \left(Z + \frac{Z^2}{2}\right) \exp\left(-Z - \frac{Z^2}{2}\right).$$

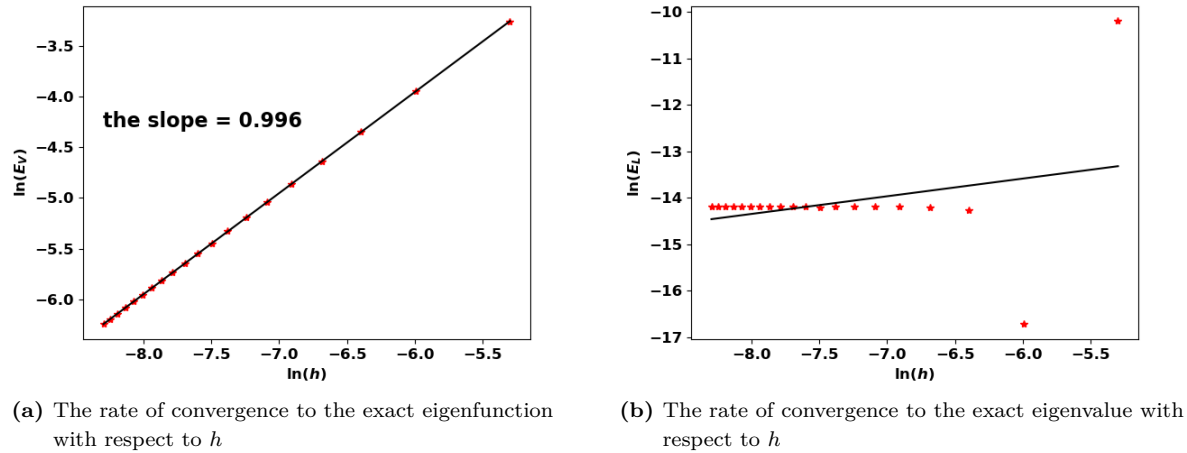


Figure 7. Binary division kernel: convergence rates of $(\lambda^{(K)}, N^{(K)})$ with respect to h

1179 We still use the values in Table 3 (especially, $a_0 = a$ and
 1180 $V_0 = V$). The approximated eigenpair is obtained in 84
 1181 iterations and, as in the previous test, it does not change
 1182 with the size step. In this case, both the eigenvalue and
 1183 the eigenfunction are approached at order 1, see Table 5
 1184 and Fig. 8.

$n = 1$	$\lambda = V_0$	$N(z) = \frac{a_0}{V_0} \exp\left(-\frac{a_0}{V_0} z\right)$
$n = 2$	$\lambda = V_0$	$N(z) = \frac{2a_0}{\pi V_0} \exp\left(-\frac{a_0}{2V_0} z^2\right)$
n	$\lambda = V_0$	$N(z) = \left(\frac{a_0}{nV_0}\right)^{\frac{1}{n}} \frac{n}{\Gamma(\frac{1}{n})} \exp\left(-\frac{a_0}{nV_0} z^n\right)$

Number of cells	E_λ	E_V
1000	1.30×10^{-2}	8.89×10^{-3}
2000	6.43×10^{-3}	4.50×10^{-3}
4000	3.23×10^{-3}	2.24×10^{-3}
8000	1.62×10^{-3}	1.13×10^{-3}

Table 5. Uniform fragmentation, ex. 1: errors for several number of grid points

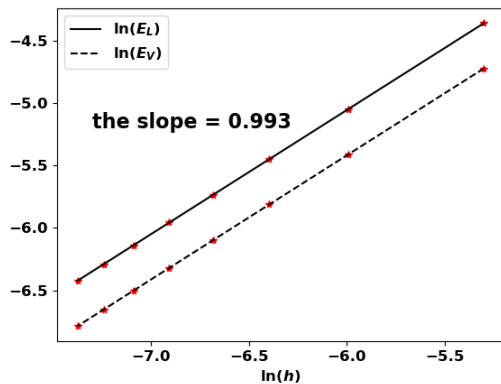


Figure 8. Uniform fragmentation, ex. 1: rate of convergence to the exact eigenpair with respect to h

1188 Note that the growth rate V vanishes and Theorem .2
 1189 does not apply as such. Nonetheless, the algorithm works
 1190 well and still captures the eigenpair. We perform the
 1191 test for $n = 1$ and $n = 2$ and the results are recorded in
 1192 Table 6, Fig. 9 and Table 7, Fig. 10, respectively.

Number of cells	E_λ	E_V
1000	4.70×10^{-2}	2×10^{-2}
2000	2.43×10^{-2}	1.06×10^{-2}
4000	1.25×10^{-2}	5.5×10^{-3}
8000	6.39×10^{-3}	2.81×10^{-3}

Table 6. Uniform fragmentation, ex. 2, case $n = 1$: errors for different number of cells

1185 2. $V(z) = V_0 z$ and $a(z) = a_0 z^n$ with $n \in \mathbb{N} \setminus \{0\}$. The
 1186 eigenpair is defined by the following formula:

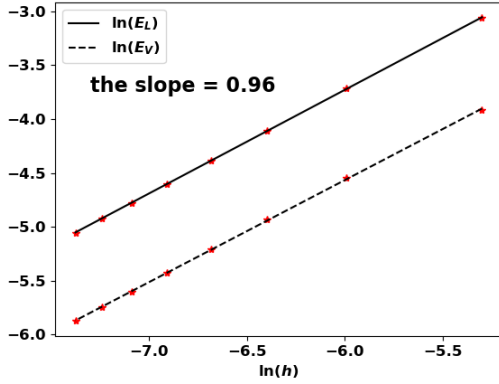


Figure 9. Uniform fragmentation, ex. 2 case $n = 1$: rate of convergence to the exact eigenpair with respect to h

Number of cells	E_λ	E_V
1000	2.39×10^{-2}	8.81×10^{-2}
2000	1.23×10^{-3}	4.53×10^{-3}
4000	6.41×10^{-4}	2.35×10^{-3}
8000	3.41×10^{-4}	1.24×10^{-3}

Table 7. Uniform fragmentation, ex. 2, case $n = 2$: errors for different number of cells

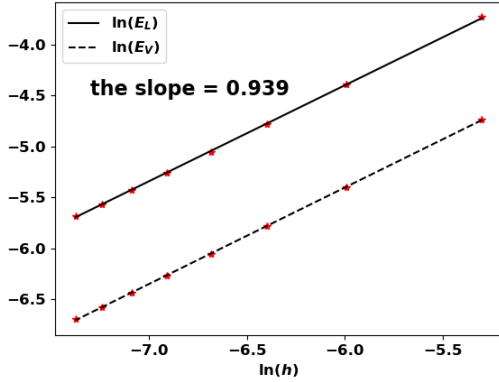


Figure 10. Uniform fragmentation, ex. 2: rate of convergence to the exact eigenpair with respect to h

Sensitivity analysis on the equilibrium mass

Having an efficient procedure to predict the residual mass of the equilibrium phase also opens perspectives to discuss the influence of the parameters. This can provide useful hints for the design and the optimization of anti-tumor therapies. We address this issue by performing a global sensitivity analysis on the immune-controlled tumor mass. Sensitivity analysis

also provides information on the quantification of uncertainty in the model output with respect to the uncertainties in the input parameters. We remind the reader that the equilibrium mass is seen as a function of the parameters in Table 1:

$$\mu_1 = f(a, A, p, \chi, D, \gamma). \quad (22)$$

We consider that the input parameters are independent random variables uniformly distributed in an interval $[x_1, x_2] \subset (0, \infty)$:

$$M = (a, A, p, \chi, D, \gamma) \text{ with } M_i \sim U(x_1, x_2). \quad (23)$$

The pillar of the Sobol sensitivity analysis is the decomposition of f into $2^n - 1$ summands of increasing dimensions:

$$f(M) = f_0 + \sum_{i=1}^n f_i(M_i) + \sum_{1 \leq i < j \leq n} f_{ij}(M_i, M_j) + \dots + f_{1\dots n}(M_1, \dots, M_n), \quad (24)$$

where

$$\frac{1}{x_2 - x_1} \int_{[x_1, x_2]} f_{i_1 \dots i_p}(M_{i_1 \dots i_p}) dM_{i_k} = 0 \quad \text{for } k \in \{1, \dots, p\}, \quad (25)$$

1212

$$f_0 = \frac{1}{(x_2 - x_1)^n} \int_{[x_1, x_2]^n} f(M) dM, \quad (26)$$

1213

$$\int_{[x_1, x_2]^n} f_{i_1 \dots i_p}(M_{i_1 \dots i_p}) f_{j_1 \dots j_p}(M_{j_1 \dots j_p}) dM = 0, \quad (27)$$

and $M_{i_1 \dots i_p} = (M_{i_1}, \dots, M_{i_p})$. The existence and uniqueness of the above decomposition has been proven in [44], given f a square integrable function. Owing to the orthogonality condition (27), the total variance of f reads:

$$\mathcal{V} = \text{Var}(f(M)) = \frac{1}{(x_2 - x_1)^n} \int_{[x_1, x_2]^n} f(M)^2 dM - f_0^2. \quad (28)$$

Given (24), \mathcal{V} can be decomposed as follows:

$$\mathcal{V} = \sum_{i=1}^n \mathcal{V}_i + \sum_{1 \leq i < j \leq n} \mathcal{V}_{ij} + \dots + \mathcal{V}_{1\dots n}, \quad (29)$$

where the terms $\mathcal{V}_{i_1 \dots i_p}$, called partial variances read:

$$\mathcal{V}_{i_1 \dots i_p} = \frac{1}{(x_2 - x_1)^n} \int_{[x_1, x_2]^n} f_{i_1 \dots i_p}^2 dM_{i_1} \dots dM_{i_p}. \quad (30)$$

Following the description in [44], the Sobol' sensitivity indices are defined as follows:

$$S_{i_1 \dots i_p} = \frac{\mathcal{V}_{i_1 \dots i_p}}{\mathcal{V}}. \quad (31)$$

They verify

$$\sum_{i=1}^n S_i + \sum_{1 \leq i < j \leq n} S_{ij} + \dots + S_{1\dots n} = 1. \quad (32)$$

1223 Each index $S_{i_1 \dots i_p}$ measures how the total variance of f is af-
 1224 fected by uncertainties in the set of input parameters $i_1 \dots i_p$.
 1225 An equivalent definition of the above indices is given by (see
 1226 [43]):

$$\mathcal{V}_i = \text{Var}(\mathbb{E}(Y|M_i)), \quad \mathcal{V}_{ij} = \text{Var}(\mathbb{E}(Y|M_i, M_j)) - \mathcal{V}_i - \mathcal{V}_j, \dots \quad (33)$$

1227 The total effect of a specific input parameter i is evaluated
 1228 by the so-called total sensitivity index $S_T^{(i)}$, the sum of the
 1229 sensitivity indices which contain i :

$$S_T^{(i)} = \sum_{C_i} S_{i_1 \dots i_p} \quad (34)$$

1230 where $C_i = \{(i_1 \dots i_p) : \exists m \in \{1, \dots, p\}, i_m = i\}$. In practice,
 1231 the sensitivity indices that are needed to discriminate the
 1232 impact of the parameters are the first, second and total Sobol'
 1233 sensitivity indices. The above indices are computed using
 1234 Monte Carlo simulations combined with a careful sampling
 1235 of the parameters space in order to reduce the computational
 1236 load and the number of model evaluations. For this purpose,
 1237 the following estimators can be derived using two different N
 1238 samples A and B , see [43, 49],

$$\hat{f}_0 = \frac{1}{N} \sum_{l=1}^N f(M_l), \quad (35)$$

$$\hat{\mathcal{V}} = \frac{1}{N} \sum_{l=1}^N f^2(M_l) - \hat{f}_0^2, \quad (36)$$

$$\hat{\mathcal{V}}_i = \frac{1}{N} \sum_{l=1}^N f(M_{(-i)l}^{(A)}, M_{il}^{(A)}) f(M_{(-i)l}^{(B)}, M_{il}^{(A)}) - \hat{f}_0^2, \quad (37)$$

$$\begin{aligned} \hat{\mathcal{V}}_{ij} &= \frac{1}{N} \sum_{l=1}^N f(M_{-(i,j)l}^{(A)}, M_{il}^{(A)}, M_{jl}^{(A)}) f(M_{-(i,j)l}^{(B)}, M_{il}^{(A)}, M_{jl}^{(A)}) \\ &\quad - \hat{f}_0^2 - \hat{\mathcal{V}}_i - \hat{\mathcal{V}}_j. \end{aligned} \quad (38)$$

1242 Here the notation $M_{-(i_1 \dots i_p)l}$ stands for the l -th sample line
 1243 where we get rid of the points corresponding to the indices
 1244 i_1, \dots, i_p . The total sensitivity [61] is given by:

$$S_{T_i} = 1 - S_{-i} \quad (39)$$

1245 where S_{-i} is the sum of all the sensitivity indices that do
 1246 not contain the index i . Hence, the total sensitivity index
 1247 estimator reads:

$$\hat{S}_{T_i} = 1 - \frac{\hat{\mathcal{V}}_{-i}}{\hat{\mathcal{V}}} \quad (40)$$

where

$$\hat{\mathcal{V}}_{-i} = \frac{1}{N} \sum_{l=1}^N f(M_{(-i)l}^{(A)}, M_{il}^{(A)}) f(M_{(-i)l}^{(B)}, M_{il}^{(B)}) - \hat{f}_0^2.$$